# Paramagnetism–assisted NMR analyses of conformational dynamics of ganglioside glycans

张　英 (Zhang Ying)

Department of Functional Molecular Science,

School of Physical Sciences,

The Graduate University for Advanced Studies (SOKENDAI)

2014 March

A dissertation submitted for the degree of Doctor of Philosophy

## Abstract:

Glycans are the carbohydrate parts of glycoconjugates such as glycoproteins, glycolipids, and proteoglycans, and mediate cell–cell communication and consequent signal transduction, thereby controlling a variety of physiological and pathological processes. For better understanding the molecular basis of the mechanisms underlying the glycan functions, it is quite desirable to gain detailed information on their conformational dynamics in solution. Hence, my thesis focuses on the development of the methodology for characterization of conformational dynamics of glycans. It consists four chapters, **Chapter 1** "General introduction," **Chapter 2** "Development of the methodology for characterization of the conformational dynamics of linear GM3 trisaccharide," **Chapter 3** "Application of paramagnetic NMR–validated molecular dynamics simulation for characterization of the conformational dynamics of branched GM2 and GM1 oligosaccharides" and **Chapter 4** "Summary and perspective."

In **Chapter 1**, I describe the general biological roles of glycans and explain the limitation of present methods for the structural analysis of glycans. Although, the glycans have important physiological and pathological roles, the conformational analysis of glycans is still a remaining challenge. This is primarily because of their dynamic conformational multiplicities and branched covalent structures, which hinder conventional analytical methods such as X–ray crystallography. Although recent advancement on computational calculation has enabled large–scale molecular dynamics (MD) simulations of oligosaccharides in solution, experimental data are indispensable for validating the simulation results because they heavily depend on the calculation conditions such as simulation time, initial state and force field. Nuclear magnetic resonance (NMR) spectroscopy has immense potential to deal with this kind of flexible biomolecules. However, the nuclear Overhauser

effect–based approach, widely used for protein structure determination, is often limited by insufficient distance–restraint information due to the low density of observable protons in glycans. For conformational characterization of dynamic glycans, their structures should not be dealt with as a single well–defined global free energy minimum but as an ensemble of low energy conformers. Hence, I have developed an NMR methodology for evaluating a dynamic ensemble of glycan conformations by employing paramagnetic effects induced by an unpaired electron, which provide long–distance information on dynamic conformations of glycans.

In **Chapter 2**, I described the structural characterization of the linear GM3 trisaccharide (αNeu5Ac–(2–3)–βGal–(1–4)–βGlc) by using the paramagnetism–assisted NMR in conjunction with MD simulation. This approach was presented to characterize the conformational dynamics of GM3 trisaccharide, which shared the common core structure among gangliosides forming an integral part of cellular membranes. To elucidate the conformations of ganglioside glycans in solution, I prepared novel phenylenediamine–based lanthanide chelating–tag. Subsequently, this phenylenediamine derivative was covalently attached to the reducing end of the chemically synthesized GM3 trisaccharide. Upon chelating with paramagnetic lanthanide ions, the tagged GM3 trisaccharide exhibited NMR spectral changes due to pseudocontact shift (PCS), thereby offering an opportunity to determine the spatial positions of the individual $^{1}H$ and $^{13}C$ nuclei with respect to the paramagnetic metal center. The PCS values of $^{1}H$ and $^{13}C$ were measured as the differences between the chemical shifts of the compound chelated to the paramagnetic ion such as $Tm^{3+}$ and those observed with the diamagnetic $La^{3+}$ ion in their $^{1}H$–$^{13}C$ heteronuclear single–quantum coherence spectra. For construction of the 3D structural model, all–atom MD simulations of the GM3 trisaccharide were employed. The observed PCS values of the trisaccharide were in excellent agreement with those back–calculated from the

conformational ensemble derived from a 120–ns MD simulation including quite minor conformers, thereby demonstrating that this methodology is useful in evaluating the multiple conformations of the linear GM3 trisaccharide in solution at atomic level.

In **Chapter 3**, I describe the application of this methodology to the analysis of conformational dynamics of the branched GM2 tetrasaccharide (βGalNAc–(1–4)–[αNeu5Ac–(2–3)]–βGal–(1–4)–βGlc), which possesses an additional GalNAc moiety in comparison with GM3 trisaccharide. The experimental PCS data were in an excellent agreement with back–calculated PCS data from the 3D ensemble model. Furthermore, the simulation results of GM1 pentasaccharide (βGal–(1–3)–βGalNAc–(1–4)–[αNeu5Ac–(2–3)]–βGal–(1–4)–βGlc) were successfully evaluated, providing the accurate conformational space of this branched oligosaccharide. These results indicated wide applicability of this methodology for analyzing the conformational dynamics of glycans. By inspecting the results of the GM1 pentasaccharide and the GM2 tetrasaccharide, I found that the outer Gal residue raised little conformational change in the GM1 pentasaccharide. By contrast, the PCS data of the Neu5Ac residues in GM3 trisaccharide and GM2 tetrasaccharide exhibited significant difference in glycosidic linkage conformation, consistent with the MD simulation results showing that different conformational space of Neu5Ac–Gal between the GM3 trisaccharide and GM2 tetrasaccharide. This result suggests that the additional GalNAc branch restricts the conformational flexibility of the Neu5Ac–Gal glycosidic linkage in the GM2 tetrasaccharide through inter–residue interactions.

In **Chapter 4,** I summarize my work and discuss the future perspective. The conformational characterization of the linear GM3 trisaccharide and the branched GM2 and GM1 oligosaccharides demonstrates that paramagnetism–assisted NMR method combined with MD simulation is useful for the conformational characterization of flexible, branched glycans. This methodology opens a new prospect for conformational analyses of dynamic

structures of ganglioside glycans toward decoding *glycocodes* from the 3D structural aspects, giving mechanistic insights into their various physiological and pathological roles in living system. However, compared to protein structural biology, the structural analyses of glycans are still immature. New NMR techniques for analyzing glycan–glycan and glycan–protein interactions and the advancement in the preparation of isotope labeled glycan samples are needed for providing elaborate information of glycans to understand their functional roles in living systems.

## Abbreviations:

3D : Three–dimensional

NMR : Nuclear Magnetic Resonance

MD : Molecular Dynamics

REMD : Replica Exchange Molecular Dynamics

NOE : Nuclear Overhauser Effect

RDC : Residual Dipolar Coupling

PRE : Paramagnetic Relaxation Enhancement

PCS : Pseudocontact Shift

$\Delta\chi$ : Anisotropic Magnetic Tensor

HSQC : Heteronuclear Single–Quantum Coherence

HRMS : High Resolution Mass Spectroscopy

FAB : Fast Atom Bombardment

$La^{3+}$ : Lanthanum Ion

$Tm^{3+}$ : Thulium Ion

$Tb^{3+}$ : Terbium Ion

TMS : Tetramethylsilane

$CDCl_3$ : Chloroform

MeOH : Methanol

DIPEA : *N,N*–Diisopropylethylamine

HATU : 1–[Bis(dimethylamino)methylene]–1H–1,2,3–triazolo[4,5–b]pyridinium 3–oxid hexafluorophosphate

DMT–MM : 4–(4,6–Dimethoxy–1,3,5–triazin–2–yl)–4–methylmorpholinium chloride

DMF : Dimethylformamide

TLC : Thin Layer Chromatography

DMSO : Dimethylsulfoxide

## Thesis Contents:

# Chapter 1: General Introduction

## 1.1 General introduction of glycans

In living systems, proteins, nucleic acids and sugar chains are the three main classes of biomacromolecules that execute and regulate life processes. The biological roles of these molecules are tightly associated with their conformations. Three–dimensional (3D) structures of a number of the biomolecules and their complexes have been revealed by using various physical techniques such as X–ray crystallography and nuclear magnetic resonance (NMR) spectroscopy [1]. However, besides the static structures, the biomolecules possess conformational motion and fluctuation in solution, as best exemplified by sugar chains. The 3D structural analysis of oligosaccharides is the most difficult case due to complexity of their structural behaviors.

Oligosaccharides, which are formed by the combination of approximately ten types of monosaccharides through various glycosidic linkages, are a major class of essential molecular components in biological systems. The anomeric carbon C1 of one monosaccharide can be linked to a second monosaccharide with two possible configurations (α and β) at either C1, C2, C3, C4 or C6 positions (for hexopyranose) and form C1–O–C1′, C1–O–C2′, C1–O–C3′, C1–O–C4′ and C1–O–C6′ glycosidic linkage, respectively [Figure 1.1]. Therefore, one sugar residue can be connected to more than two sugar residues. This multiple linkages generate diverse branched structures of oligosaccharides unlike polypeptides. [2].

These glycosidic linkages in oligosaccharides have high–level motional ability due to the flexible C–O–C bond. Two torsion angles Φ and Ψ are mainly employed to describe the conformation of the glycosidic linkages [Figure 1]. The torsion angles Φ and Ψ is defined as (for instance, for galactose–glucose linkage of the pentasaccharide in Figure 1): Φ = GalH1–GalC1–GlcO4–GlcC4, and Ψ = GalC1–GalO4–GlcC4–GlcH4. The Φ torsion angle is largely affected by stereoelectronic factors called as exo–anomeric effect, involving the lone pairs on

the linkage oxygen. The exo–anomeric effect governs the torsion angle Φ and favors gauche conformations. On the other hand, the Ψ torsion angle is dominantly determined by the steric interactions between the sugar residues. The repulsive steric hindrance usually cause disaccharides prefer to have a staggered conformation rather than an eclipsed conformation. In addition, these preferences can be superseded by hydrogen bonds between residues and with the solvent [2a, 3].

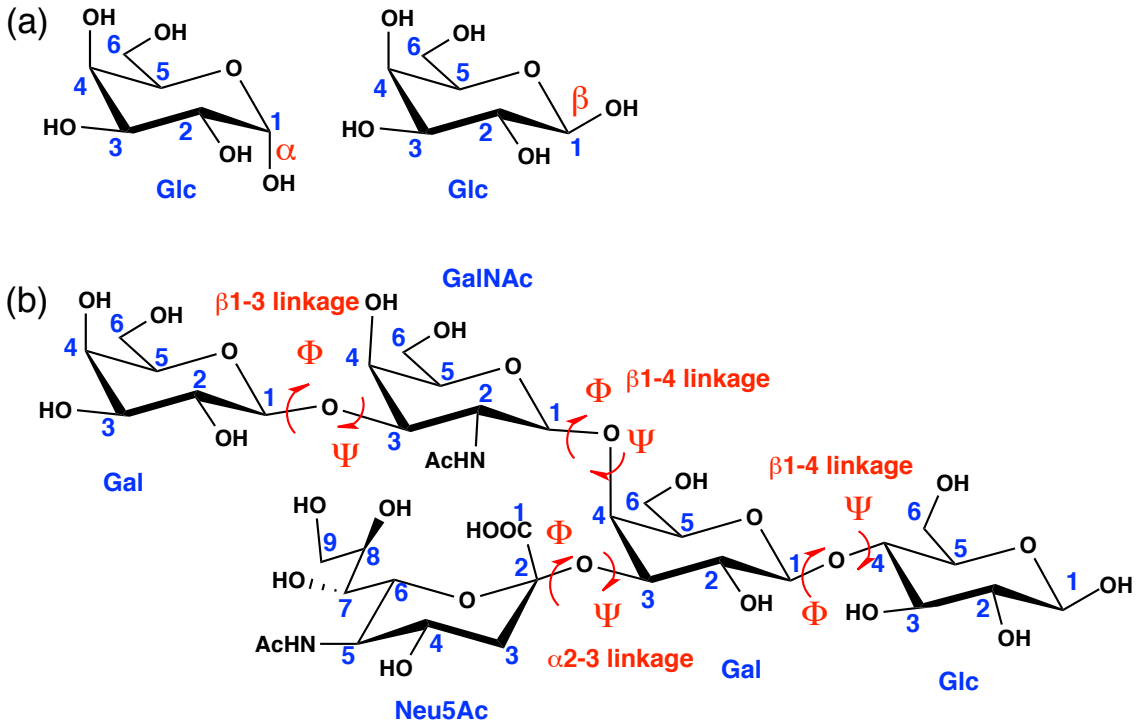


**Figure 1.1**. (a) α and β configuration of glucose. (b) Schematic diagrams of a pentasaccharide of GM1 ganglioside (βGal–(1–4)–βGalNAc–(1–4)–[αNeu5Ac–(2–3)]–βGal–(1–4)–βGlc), showing the torsion angles (Φ, Ψ) of the glycosidic linkages [glucose (Glc); galactose (Gal), *N*–acetylneuraminic acid (Neu5Ac), *N*–acetylgalactosamine (GalNAc)]

The numerous connections and large conformational space of the glycosidic linkage provide significant degree of motional freedom of oligosaccharides, thereby exhibiting conformational adaptability upon interacting with various target molecules in molecular recognition systems. This highly branching and flexible structure enables oligosaccharides

serve as mediators in physiological and pathological events by modifying proteins and lipids. Oligosaccharide covalently connected to proteins or lipids is called as glycan. Glycans are involved in a wide range of cellular processes including protein–fate determination, intercellular communication, and viral infections [4]. Therefore, atomic descriptions of dynamic glycan conformations are important not only for understanding the quantitative energetics of carbohydrate–protein and carbohydrate–carbohydrate interactions but also for designing drugs targeting these interacting systems. However, compared to protein structural biology, conformational dynamics analysis of oligosaccharides is still immature. The inherent flexibility makes the structural analysis of oligosaccharides difficult by traditional techniques such as crystallography. Hence, theoretical approaches such as computational simulation and experimental studies including NMR have been proposed to solve this long–standing issue of conformational analysis of oligosaccharides (*vide infra*).

## 1.2 Conventional methods for structural analysis of glycans

### 1.2.1 Molecular dynamics simulation of glycans

Computational simulation is a technique that explores the macroscopic properties of a system through microscopic simulation. Molecular dynamics (MD) simulation is one of the powerful molecular simulation technique that provide detailed information of the fluctuations and conformational changes of flexible biomolecules through calculating the time dependent behavior of the molecular system [5]. MD simulation is a technique that creates the atomic trajectories of the system by integrating Newton's equations of motion for all atoms with a specific potential existing between the atoms. In contrast to experimental data, where the obtained information is the average of the motions in a time range, molecules can be allowed to move and interact according to Newton's second law of motion over a period of time in MD simulations.

For getting appropriate simulation results, a force field is one of most important factor that refers to the form and parameters of the mathematical function of the potential energy used to describe the relationship of the structure to the energy of the system. During the past decades, many progresses have been made to improve the force fields for proteins, nucleic acids and lipids [6]. However, the force field for carbohydrates is more complicated due to the distinctive structures of sugar chains possessing diverse glycosidic linkages [7]. In addition, only limited experimental data of oligosaccharides have been available for the force field refinement. Because of these difficulties, the force field improvements for carbohydrates have been lagged behind compared with other biomolecules. One of the recently developed force field for carbohydrates is GLYCAM force field generated by considering their unique properties [8].

Although recent advancements in computational approaches have enabled large–scale MD simulations in solution with the improved force field, simulation results of complicated oligosaccharides still depend on the simulation time and the initial structure. Additionally, the conformational space of oligosaccharide involves multiple minima separated by distinct energy barriers. Therefore, extensive conformational sampling is required to access multiple conformers of oligosaccharides [9]. Hence, experimental data for validating the simulation result are indispensable. However, the experimental methodology to evaluate the conformational dynamics of oligosaccharides has not yet been fully developed.

### 1.2.2 Conventional NMR methods for glycans

NMR is the only experimental method, which can provide the atomic 3D structural information of flexible biomolecule in solution. Several conventional NMR approaches such as nuclear Overhauser effects (NOE) and spin–spin coupling (*J* coupling) [10], have been

tried to obtain the structural information of inter–residue arrangements for characterizing the 3D structure of oligosaccharides.

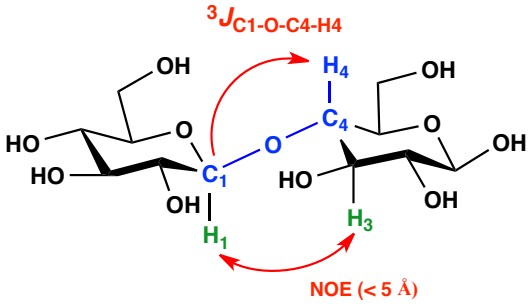


**Figure 1.2**. Inter–residue NOE and *J* coupling measurements

NOE originates from the dipole–dipole interaction between two nuclei. The magnitudes of NOE are inversely proportional to distance of two nuclei of the sixth power ($1/r^6$). NOE is an extensively used NMR technique for structural analysis of biomolecules by providing the spatial distance information of two protons that are close to each other in 5 Å [11]. However, only low number of inter–residue NOEs can be obtained due to the low–proton density of oligosaccharides.

*J* coupling comes from the indirect interaction between two nuclear spins with the aid of bonding electron. The coupling constant depends on the bond length and angle. Although inter–residue *J* coupling, i.e. $^3J_{C,H}$ can provide the structural restraint according to the torsion angles of the glycosidic linkage [12], the coupling constants are often too small to precise definition of the oligosaccharide conformations. Furthermore, NOE and *J* coupling are not enough to understand the overall conformations of oligosaccharides because these values only provide short distance information describing local structures. Hence, for obtaining sufficient 3D structural information to characterize the conformational dynamics of oligosaccharides, novel NMR approaches that can provide long–distance restraint are desired.

## 1.3 Paramagnetic effect

In addition to the dipole–dipole interactions between nuclear spins, electron spins also perturb NMR signals of the nuclei according to their spatial arrangements. Paramagnetism–assisted NMR approaches, involving the introduction of a paramagnetic center, for example a paramagnetic ion or a nitroxide radical, into a target biomolecule, provide information about the geometric arrangement of nuclei through long–distance magnetic dipole–dipole interactions between nuclei and an unpaired electron and/or weak molecular alignment in the magnetic field [13]. The three kinds of paramagnetic effects that often utilized are referred to as residual dipolar coupling (RDC), paramagnetic relaxation enhancement (PRE) and pseudocontact shift (PCS) [Figure 1.3]. The great attractive properties of these three paramagnetic effects lie in their capability of providing long–distance structural restraints. Especially, PCS can reach as far as 40 Å from the paramagnetic probe.

### 1.3.1 Origin of PCSs

The interaction between unpaired electron and NMR nucleus induces chemical shift perturbation called as hyperfine shift [14]. Hyperfine shift consist of two contributions, contact shift and PCS [15].

$$\delta^{hf} = \delta^{con} + \delta^{pcs}$$

The chemical shift change caused by the interaction between the unpaired electron spin and the NMR nuclei through the chemical bond is called contact shift or Fermi contact shift. Although contact shift also depends on the bond length and angle, this specific phenomenon can only be observed within very short distance (approximate 4 Å) around the paramagnetic center.

PCS is the paramagnetic effect that occurs through space dipole–dipole interaction between the unpaired electron of the paramagnetic center and the nuclei. PCS value is

inversely proportional to the cube of the distance between the nuclei and the paramagnetic center [Figure 1.3], and thus can reach the nuclei far from the unpaired electron up to 40 Å.

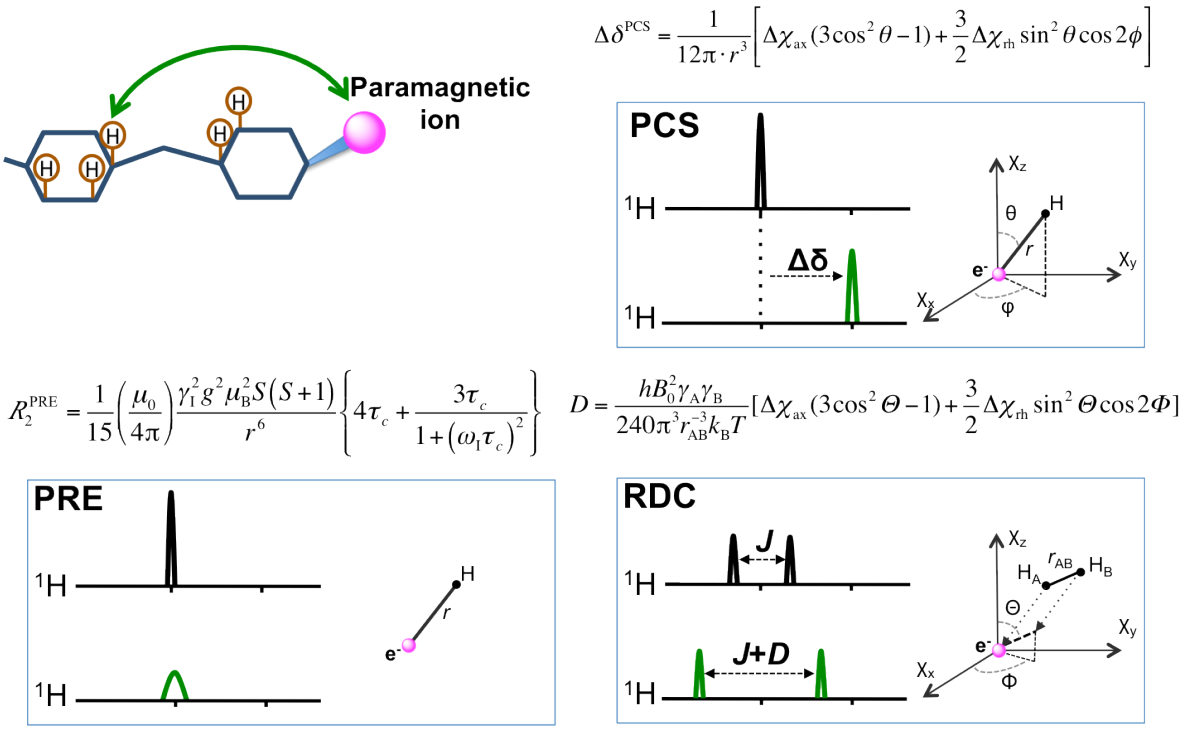


**Figure 1.3**. Observation of paramagnetic effects in NMR for the confomational analysis of oligosaccharides. $\Delta\chi_{ax}$ and $\Delta\chi_{rh}$ are the axial and rhombic components, respectively, of the anisotropic magnetic susceptibility ($\Delta\chi$) tensor. In the equation for PCS, $r$, $\theta$, and $\Phi$ are the polar coordinates of the nucleus with respect to the paramagnetic center and the principal axis of the $\Delta\chi$ tensor. Transverse relaxation enhancement through dipole–dipole interactions is described by the equation shown, where $\mu_0$ is the permeability of vacuum; $\gamma_I$ is the gyromagnetic ratio of the nucleus; $\omega_I/2\pi$ is the Larmor frequency of the nucleus; $g$, $\mu_B$, and $S$ are the electronic g–factor, Bohr magneton, and spin, respectively; $r$ is the distance between the paramagnetic center and the nucleus; and $\tau_c$ is the correlation time, defined as $1/\tau_c = 1/\tau_r + 1/\tau_e$, where $\tau_r$ and $\tau_e$ are the rotational correlation times of the molecule and the effective electron relaxation time, respectively. In the equation for RDC, $h$ is Planck's constant, $B_0$ is the magnetic field strength, $k$ is the Boltzmann constant, and $T$ is temperature. $\gamma_A$ and $\gamma_B$ are the gyromagnetic ratios of nuclei A and B, respectively. $r_{AB}$, $\Theta$, and $\Phi$ describe the internuclear vector in the principal axes system of the alignment tensor. Reproduced from Zhang. Y, et. al. *Chem. Lett*. 42 (**2013**) 1455-1462 with permission from The Chemical Society of Japan.

The paramagnetic effect originating from a single paramagnetic center is most easily described in terms of the magnetic susceptibility tensor (χ tensor), which shows the interaction between magnetic dipolar moment of unpaired electron and external magnetic field [16]. χ tensor can be divided into isotropic component and anisotropic component (Δχ tensor) due to the deviation of the χ tensor from the spherical symmetry [17]. Based on three principal axes, $\chi_x$, $\chi_y$, and $\chi_z$ of χ tensor, the Δχ tensor can be expressed as axial and rhombic components:

$\Delta\chi_{ax} = \chi_z - (\chi_x + \chi_y)/ 2$ and $\Delta\chi_{rh} = \chi_x - \chi_y$

Δχ tensor will be equal to zero, if the $\chi_x = \chi_y = \chi_z$. The coordination environment of the paramagnetic ions governs their Δχ tensors.

χ tensors determine the paramagnetic effects observable in the system. PRE can be detected in any paramagnetic system, but RDC and PCS can be detected only in the presence of Δχ tensor [Figure 1.3]. Due to the long–distance restraints that PCS provides, application of PCS is the potentially appropriate method for the experimental approaches of conformational dynamics of flexible oligosaccharides.

### 1.3.2 Paramagnetic probes for PCS measurement

PCSs are measured as the difference of chemical shift of the molecules between in the diamagnetic and paramagnetic state. Lanthanide ions and transition metal ions contain diamagnetic ions and paramagnetic ions with Δχ tensor, benefiting for the PCS measurements. The diamagnetic ion is essential for deduction of the possible chemical shift change caused by metal binding. Owing to multiple kinds of lanthanide ions compared with transition metal ions and the similar ionic radii of diamagnetic and paramagnetic lanthanide ions that can reduce the difference caused by ion binding, lanthanide ions are widely used as the paramagnetic probe for PCS measurements. According to the magnitude of Δχ tensor,

lanthanide ions have been classified into: high paramagnetic ($Dy^{3+}$, $Tb^{3+}$ and $Tm^{3+}$), moderately paramagnetic ($Er^{3+}$ and $Yb^{3+}$), little paramagnetic ($Eu^{3+}$, $Ce^{3+}$ and $Sm^{3+}$) and diamagnetic ($La^{3+}$ and $Lu^{3+}$) [16]. $Tm^{3+}$ is widely used as the paramagnetic ion for the PCS analyses of biomolecules due to the large $\Delta\chi$ and acceptable PRE that often induces unfavorable peak disappearances. The similar ionic radii of $La^{3+}$ ion and $Tm^{3+}$ ion makes $La^{3+}$ ion as the suitable diamagnetic reference for PCS observation.

## 1.4 Scope of this study

### 1.4.1. Development of the methodology for conformational dynamics analyses of glycans

The high flexibility of oligosaccharides makes it difficult to characterize their overall conformations by using conventional NMR techniques such as NOE and *J* coupling. PCS can provide long distance restraints, which is valuable to obtain the 3D structural information of flexible oligosaccharides. However, experimental data is generally the average of all conformers in solution. Such data should be interpreted as the dynamic conformational ensemble instead of one averaged conformer or the minimum energy conformer. On the other hand, MD simulation is powerful to provide the 3D structural ensemble of flexible biomoleucles, but simulation results usually depend on the force field, simulation time, initial structures and/or other parameters. Hence, experimental data for validating the simulation results is indispensable. Based on these situations, I propose the development of a systematic methodology by the combination of PCS observation and MD simulation to elucidate the conformational dynamics of flexible oligosaccharides (Scheme 1.1). For constructing the methodology, ganglioside glycans were used as the model oligosaccharides.

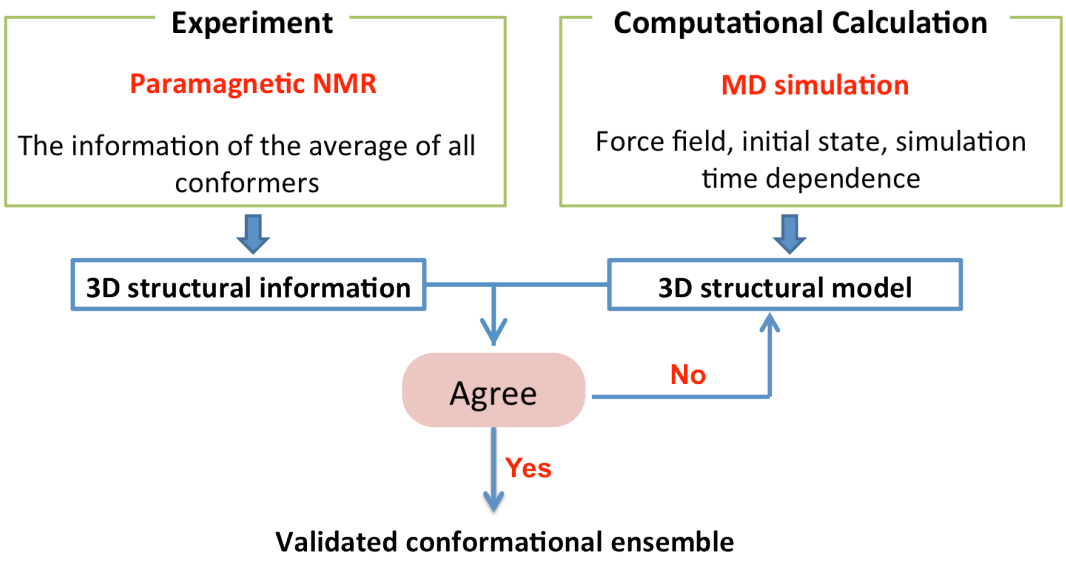


**Scheme 1.1.** Development of methodology for oligosaccharide conformational dynamics analyses by employing MD simulation in conjunction with paramagnetic NMR.

### 1.4.2. Gangliosides

Gangliosides, sialylated glycosphingolipids, act as the key components of animal cell membranes particularly in the central nervous system and play various physiological and pathological roles as receptors for microbial toxins, mediators of cell adhesion and modulator of signal transduction [18]. Significant examples provided by GM1 ganglioside which is composed of a branched pentasaccharide (βGal–(1–4)–βGalNAc–(1–4)–[αNeu5Ac–(2–3)]–βGal–(1–4)–βGlc) [Figure 1.1] are the interaction with cholera toxin, polyoma virus, growth–regulatory galectin–1 and autoantibodies associated with Guillain–Barré syndrome [19]. Spectroscopic characterization of the interaction between amyloid β (Aβ) protein and GM1 in its micellar form indicated that the GM1 clusters paly important role for accommodation and subsequent structural change of Aβ, which is supposed to be a crucial step for Aβ aggregation on cell membrane relating to Alzheimer's disease [20].

The diverse 3D structure of the GM1 pentasaccharide in micelles [20] and in the complexes with cholera toxin [19a], polyoma virus [19b] visualized by NMR and X–ray crystallographic analyses suggested that the GM1 pentasaccharide show conformational

adaptability upon binding to proteins in receptor–dependent manners [Figure 1. 4]. Hence, to understand the mechanisms of various biological roles of ganglioside glycans behind the highly flexible structures, it is crucial to elucidate the dynamic ensemble of their conformations.

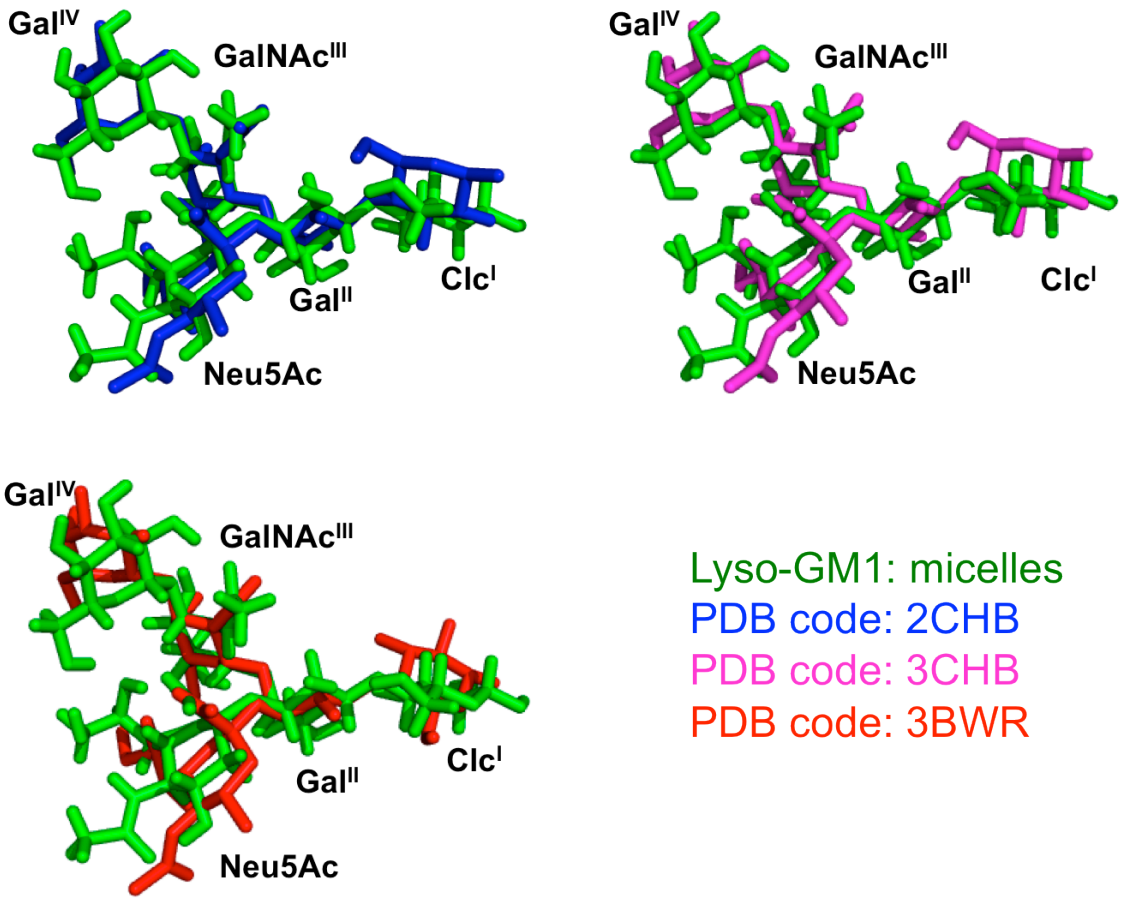


**Figure 1.4.** Comparison of the 3D structures of the pentasaccharide moieties of GM1 in micelles (green) with those complexed with cholera toxin (PDB codes: 2CHB (blue) and 3CHB (magenta)) or with simian virus 40 (PDB code: 3BWR (red)). This Figure was originally from Yagi. M **(2010)** PhD thesis, Nagoya City University, Japan.

In addition to GM1, GM2 and GM3 which possess tetra– and trisaccharide respectively, a series of typical gangliosides, are also functioning molecules in living system. GM3, GM2 and GM1 share the common core glycan structure among all gangliosides

[Figure 1.5]. Recently, the interactions between α–synuclein, an intrinsically disordered protein involved in Parkinson's disease, and GM1 or GM2 clusters, but not GM3 were reported, demonstrating that specific recognition events between gangliosides and intrinsically disordered proteins associated with neural dysfunction [21]. Furthermore, gangliosides have close relationship with cell growth factor. For example, GM1 and GM2 inhibited basic–fibroblast–growth–factor (bFGF)–induced bovine aortic endothelial cells growth, whereas GM3 acted synergistically with bFGF to enhance endothelial–cell proliferation [22]. GM2/GM3 complex interacts with tetraspanin CD82 and then interact with Met and thereby inhibits hepatocyte growth factor–induced Met tyrosine kinase activity, while single GM3 shows no impact to this system [23]. To know how these gangliosides function in living system, it is important to characterize their dynamic conformational differences at atomic level.

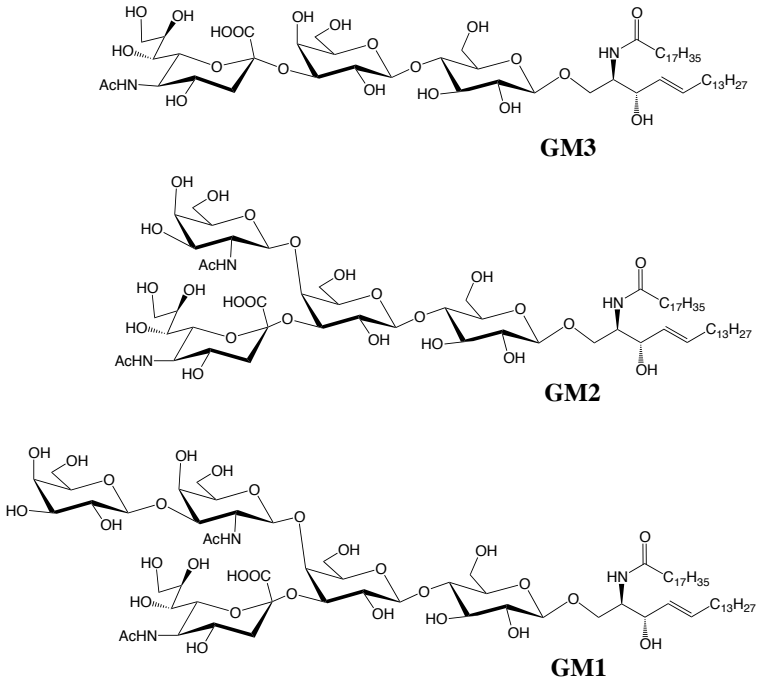


**Figure 1.5**. Ganglioside GM3, GM2 and GM1

### 1.4.3 Analyses of the conformational dynamics of ganglioside glycans

By connecting a lanthanide ion binding tag to the reducing terminal of oligosaccharides, the PCS data can be detected through NMR measurements of the oligosaccharide binding with diamagnetic and paramagnetic ions. Firstly, I developed the methodology for analyzing the conformational dynamics of glycans by using GM3 trisaccharide as a model oligosaccharide. A newly designed lanthanide ion binding tag was attached to the reducing terminal of GM3 trisaccharide. The PCS was successfully obtained by performing NMR measurements with diamagnetic ion ($La^{3+}$) and paramagnetic ion ($Tm^{3+}$ or $Tb^{3+}$) binding GM3 trisaccharide. Experimentally obtained PCSs have outstanding agreement with the back–calculated PCS data form the 3D structural ensemble model including quite minor conformers of the trisaccharide generated by MD simulations. The results showed that this methodology can visualize the conformational dynamics of linear GM3 trisaccharide.

For ensuring the applicability of this methodology, the conformational dynamics of branched GM2 tetrasaccahride and GM1 pentasaccharide were analyzed by the paramagnetism–assisted NMR in conjunction with MD simulation. The experimental data of these glycans were in a great agreement with back–calculated PCS data from the 3D ensemble models, providing the accurate conformational spaces of the branched oligosaccharides. In addition, I found the inter–branch interactions that are responsible for the unique conformation of the glycosidic linkage in the branching structure of GM2 tetrasaccahride and GM1 pentasaccharide.

Through the study of my thesis, the systematic methodology for elucidating the conformational dynamic ensemble of flexible oligosaccharides was successfully developed. The experimental PCS data is valuable for validating the simulation results. This methodology opens a new prospect for conformational analyses of dynamic structures of oligosaccharides towards decoding *glycocodes* from the 3D structural aspects.

## Reference:


1. **(a)** M. R. Wormald, A. J. Petrescu, Y. L. Pao, A. Glithero, T. Elliott and R. A. Dwek, Conformational studies of oligosaccharides and glycopeptides: complementarity of NMR, X–ray crystallography, and molecular modelling. *Chem. Rev.,* 102 **(2002)** 371–386. **(b)** Y. Kamiya, M. Yagi–Utsumi, H. Yagi and K. Kato, Structural and molecular basis of carbohydrate–protein interaction systems as potential therapeutic targets. *Curr. Pharm. Des.,*17 (**2011**) 1672–168.
2. **(a)** M. R. Wormald, A. J. Petrescu, Y. L. Pao, A. Glithero, T. Elliott, and R. A. Dwek, Conformational studies of oligosaccharides and glycopeptides: complementarity of NMR, X–ray crystallography, and molecular modelling, *Chem. Rev.,* 102 (**2002**) 371–386. **(b)** A. Varki, R. D. Cummings, J. D. Esko, H. H. Freeze, P. Stanley, C. R. Bertozzi, G. W. Hart, and M. E. Etzler, Essentials of Glycobiology, 2nd edition, *Cold Spring Harbor (NY): Cold Spring Harbor Laboratory Press*; **2009**.
3. K. Kato and Y. Yamaguchi, Glycoproteins and antibodies: solution NMR studies, encyclopedia of magnetic resonance, *John Wiley & Sons, Ltd.* **2007–2011.**
4. **(a)** A. Varki, Biological roles of oligosaccharides: all of the theories are correct. *Glycobiology*, 3 (**1993**) 97–130. **(b)** K. Kato, Y. Kamiya, Structural views of glycoprotein–fate determination in cells, *Glycobiology* 17 (**2007**) 1031–1044.
5. D. C. Rapaport, The art of molecular dynamics simulation, *Cambridge University Press*, **2004**.
6. D. A. MacKerell, Empirical force fields for biological macromolecules: overview and issues, *J. Comput. Chem*. 25 (**2004**)1584–1604.
7. **(a)** R. U. Lemieux, S. Koto, D. Voisin, Anomeric effect: origin and consequences. In ACS Symposium Series No. 87, ed. W. A. Szarek, D. Horton editors, *Washington, DC:*

*Am. Chem. Soc*. **1979. (b)** A. J. Kirvy, The anomeric effect and related stereoelectronic effects at oxygen. *Berlin: Springer–Verlag*, **1983.**

8. **(a)** R. J. Woods, R. A. Dwek, C. J. Edge, B. Fraser–Reid, Molecular mechanical and molecular dynamical simulations of glycoproteins and oligosaccharides. 1. GLYCAM–93 parameter development, *J Phys Chem* 99 (**1995**) 3832–3846. **(b)** M. Basma, S. Sundara, D. Calgan, T. Vernali, R. J. Woods, Solvated ensemble averaging in the calculation of partial atomic charges, *J Comput Chem* 22 (**2001**) 1125–1132. **(c)** K. N. Kirschner, R. J. Woods, solvent interactions determine carbohydrate conformation, *Proc Natl Acad Sci USA* 98 (**2001**) 10541–10545.
9. L. Perić–Hassler, H. S. Hansen, R. Baron, P. H. Hünenberger, Conformational properties of glucose–based disaccharides investigated using molecular dynamics simulations with local elevation umbrella sampling. *Carbohyd Res* 345(**2010**) 1781–1801. (b) S. Re, W. Nishima, N. Miyashita, Y. Sugita, Conformational flexibility of N–glycans in solution studied by REMD simulations, *Biophys Rev* 4 (**2012**) 179–187.
10. J. F. G Vliegenthar, R. J. Woods, NMR spectroscopy and computer modeling of carbohydrates, *Am. Chem. Soc* (**2006**).
11. **(a)** D. Neuhaus, M. Williamson, The nuclear Overhauser effect in structural and conformational analysis. *New York:VCH*, **1989**. **(b)** M. Zierke, M. Smiesko, S. Rabbani, T. Aeschbacher, B. Cutting, F. H. T. Allain, M. Schubert and B. Ernst, Stabilization of branched oligosaccharides: lewisx benefits from a nonconventional C−H···O hydrogen bond, *J. Am. Chem. Soc*. 135 (**2013**) 13464−13472.
12. **(a)** K. Hanna, M. Jonsson, E. Säwén and G. Widmalm, Studies on the conformational flexibility of α–L–rhamnose–containing oligosaccharides using $^{13}$C–site–specific labeling, NMR spectroscopy and molecular simulations: implications for the three–dimensional structure of bacterial rhamnan polysaccharides, *Org. Biomol. Chem*., 10

(**2012**) 2453−2463. **(b)** B. Bose, S. Zhao, R. Stenutz, F. Cloran, P. B. Bondo, G. Bondo, B. Hertz, I. Carmichael, A. S. Serianni, Three–bond C–O–C–C spin–coupling constants in carbohydrates: development of a Karplus relationship, *J. Am. Chem. Soc.* 120 (**1998**) 11158–11173. **(c)** H. Zhao, I. Carmichael, A. S. Aerianni, Oligosaccharide trans–glycoside $^{3}J_{COCC}$ Karplus curves are not equivalent: effect of internal electronegative substituents, *J. Org. Chem.* 73 (**2008**) 3255–3257.

13. I. Bertini, C. Luchinat, G. Parigi, Magnetic susceptibility in paramagnetic NMR, *Prog. Nucl. Magn. Reson. Spectrosc.,* 40 (**2002**) 249–273.
14. P. Comba, Modeling of molecular properties, *John Wiley & Sons*, **2011**.
15. K. Wuthrich, NMR in biological research: peptides and proteins, *American Elsevier Pub. Co.,* **1976**.
16. G. Otting, Prospects for lanthanides in structural biology by NMR, *J Biomol NMR* 42 (**2008**) 1–9.
17. G. Otting, Protein NMR using paramagnetic ions, *Annu. Rev. Biophys.* 39 (**2010**) 387–405.
18. **(a)** S. Hakomori, Carbohydrate–to–carbohydrate interaction, through glycosynapse, as a basis of cell recognition and membrane organization. *Glycoconj J* 21 (**2004**) 125–37. **(b)** P. H. Lopez, R. L. Schnaar, Gangliosides in cell recognition and membrane protein regulation. *Curr Opin Struct Biol* 19 (**2009**) 549–57.
19. **(a)** J. Hölmgren, I. Lönnroth, J. Månsson, L. Svennerholm, Interaction of cholera toxin and membrane GM1 ganglioside of small intestine. *Proc Natl Acad Sci USA* 72 (**1975**) 2520–2524. **(b)** U. Neu, K. Woellner, G. Gauglitz, T. Stehle, Structural basis of GM1 ganglioside recognition by simian virus 40. *Proc Natl Acad Sci USA* 105 (**2008**) 5219–5224. **(c)** J. Kopitz, C. von Reitzenstein, M. Burchert, M. Cantz, H. J. Gabius, Galectin–1 is a major receptor for ganglioside GM1, a product of the growth–

controlling activity of a cell surface ganglioside sialidase, on human neuroblastoma cells in culture. *J Biol Chem* 273 (**1998**) 11205–11211. **(d)** N. Yuki, Carbohydrate mimicry: a new paradigm of autoimmune diseases. *Curr Opin Immunol* 17 (**2005**) 577–582.

20. **(a)** M. Yagi–Utsumi, T. Kameda, Y. Yamaguchi, K. Kato, NMR characterization of the interactions between lyso–GM1 aqueous micelles and amyloid beta*, FEBS Lett.*, 584 (**2010**) 831–836. **(b)** M. Utsumi, Y. Yamaguchi, H. Sasakawa, N. Yamamoto, K. Yanagisawa, K. Kato, Up–and–down topological mode of amyloid β–peptide lying on hydrophilic/hydrophobic interface of ganglioside clusters, *Glycoconjugate J.* 26 (**2009**) 999–1006.

21. T. Yamaguchi, T. Uno, Y. Uekusa, M. Yagi–Utsumi, K. Kato, Ganglioside–embedding small bicelles for probing membrane–landing processes of intrinsically disordered proteins, *Chem. Commun.* 49 (**2013**) 1235–1237.

22. M. Slevin, S. Kumar, X. He, J. Gaffney, Physiological concentrations of gangliosides GM1, GM2 and GM3 differentially modify basic–fibroblast–growth–factor–induced mitogenesis and the associated signalling pathway in endothelial cells, *Int J Cancer*, 82 (**1999**) 412–23

23. **(a)** A. R. Todeschini, J. N. Dos Santos, K. Handa, S. I. Hakomori Ganglioside GM2/GM3 complex affixed on silica nanospheres strongly inhibits cell motility through CD82/cMet–mediated pathway, *Proc Natl Acad Sci U S A.* 105 (**2008**) 1925–1930. **(b)** A. R. Todeschini, J. N. D. Santos, K. Handa, and S. Hakomori, Ganglioside GM2–tetraspanin CD82 complex inhibits Met and its cross–talk with integrins, providing a basis for control of cell motility through glycosynapse, *J Biol Chem* 282 (**2007**) 8123–8133.

# Chapter 2: Development of the methodology for characterization of the conformational dynamics of linear GM3 trisaccharide

This chapter is adapted and modified from Sayoko Yamamoto, Ying Zhang, Takumi Yamaguchi, Tomoshi Kameda and Koichi Kato, Lanthanide–assisted NMR evaluation of a dynamic ensemble of oligosaccharide conformations, Chemical Communications, 2012, 48, 4752–4754.

## 2.1 Introduction

Oligosaccharides possess significant degrees of motional freedom, exhibiting conformational adaptability upon interacting with various target molecules in molecular recognition events [1]. Therefore, atomic descriptions of dynamic oligosaccharide conformations are important not only for understanding the quantitative energetics of carbohydrate–protein and carbohydrate–carbohydrate interactions but also for designing drugs targeting these interacting systems [2]. Although recent advancements in computational approaches have enabled large–scale MD simulations of oligosaccharides in solution with improved force fields, the simulation results often depend on the initial state and/or simulation time [3]. Therefore, the experimental data for validating the simulation results has been indispensible. In this chapter, for analyzing the conformational dynamic ensemble of flexible oligosaccharides quantitatively, a systematic methodology was designed by employing PCS in conjunction with MD simulations.

One of the appropriate choices for obtaining experimental data of flexible oligosaccharides is PCS, which can reach the atoms 40 Å far away form the paramagnetic center [4]. For observing of PCSs successfully, the lanthanide ion must be site–specifically connected to the biomolecule of interest. The easy way to incorporate the lanthanide ion to metalloprotein is to replace physiological ion such as the $Ca^{2+}$, $Mg^{2+}$, $Mn^{2+}$ ions with lanthanide ions [5]. For ensuring the site–specific lanthanide labeling of proteins, several techniques have been developed by fusing lanthanide–binding peptides to the N– or C–terminal of proteins [6] or forming a covalent bond between the tag and a thiol group of the target protein to achieve paramagnetic labeling [7]. Although this method has been employed for structural analyses of several proteins [8], until recently, it has not been applied to carbohydrate NMR spectroscopy probably because of the lack of a conventional method to attach lanthanide ions to oligosaccharides [9]. For oligosaccharides conformational analyses,

a well–designed lanthanide tag is essential. The rigidity of the tag as well as the stability of the lanthanide complex is crucial factors for unambiguous interpretation of the PCS data. In view of this situation, a novel phenylenediamine based lanthanide chelating–tag was designed (shown in scheme 2.1). This phenylenediaminetetraacetic acid derivative is applied to chelate metal ions. The rigid benzene ring was inserted to suppress the unfavorable relaxation enhancement and contact shift of the carbohydrate resonances originating from the nuclei, which are closed to the coordinated paramagnetic center. The carboxy group connecting with phenylene spacer is used to link the tag with the reducing end of oligosaccharides. By virtue of this tag, I herein attempt to combine the lanthanide–assisted NMR method with MD simulations for the evaluation of dynamic conformational ensembles of highly flexible oligosaccharides that exhibit shallow and broad energy minima in their conformational space.

## 2.2 Results and Discussion

### 2.2.1 Analyses of PCS data

GM3 trisaccharide αNeu5Ac–(2–3)–βGal–(1–4)–βGlc was used as a model oligosaccharide due to the common core structure shared among gangliosides. The key to lanthanide tagging is to introduce a metal–chelating unit to the reducing end of the oligosaccharide, which can form a stable complex with a paramagnetic lanthanide ion. A phenylenediamine–based lanthanide–chelating tag was newly designed to improve the rigidity of the tag, which is crucially important for the accurate interpretation of PCS data in terms of carbohydrate dynamics. This novel tag was successfully attached to the trisaccharide, as shown in Scheme 2.1. The reducing terminus of the sugar moiety was selectively aminated in good yield; subsequently, it was connected to the tag through an amide linkage. By $^{1}$H NMR titration experiments, it was confirmed that the lanthanide ions

were selectively bound to the tag moiety of the trisaccharide, giving rise to a stable 1:1 complex.

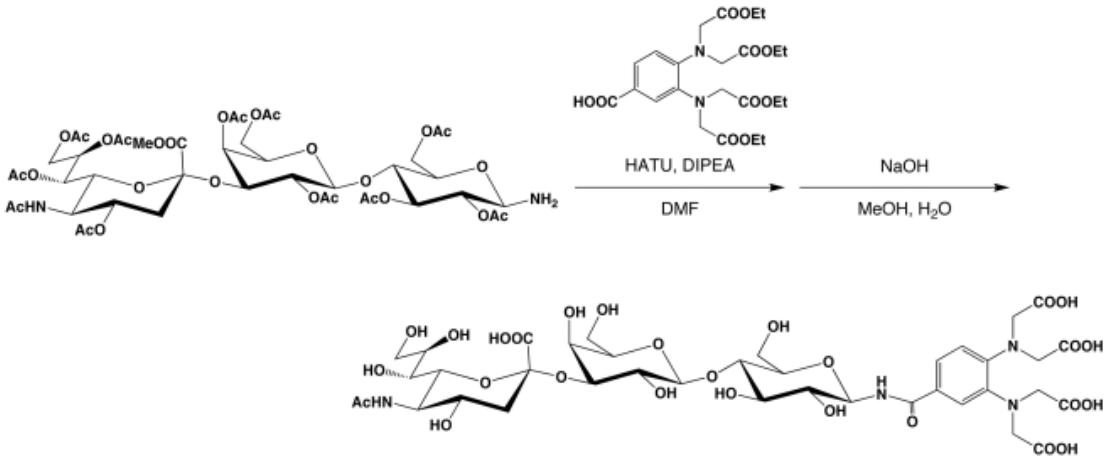


**Scheme 2.1**. Introduction of the lanthanide–chelating tag into the GM3 trisaccharide

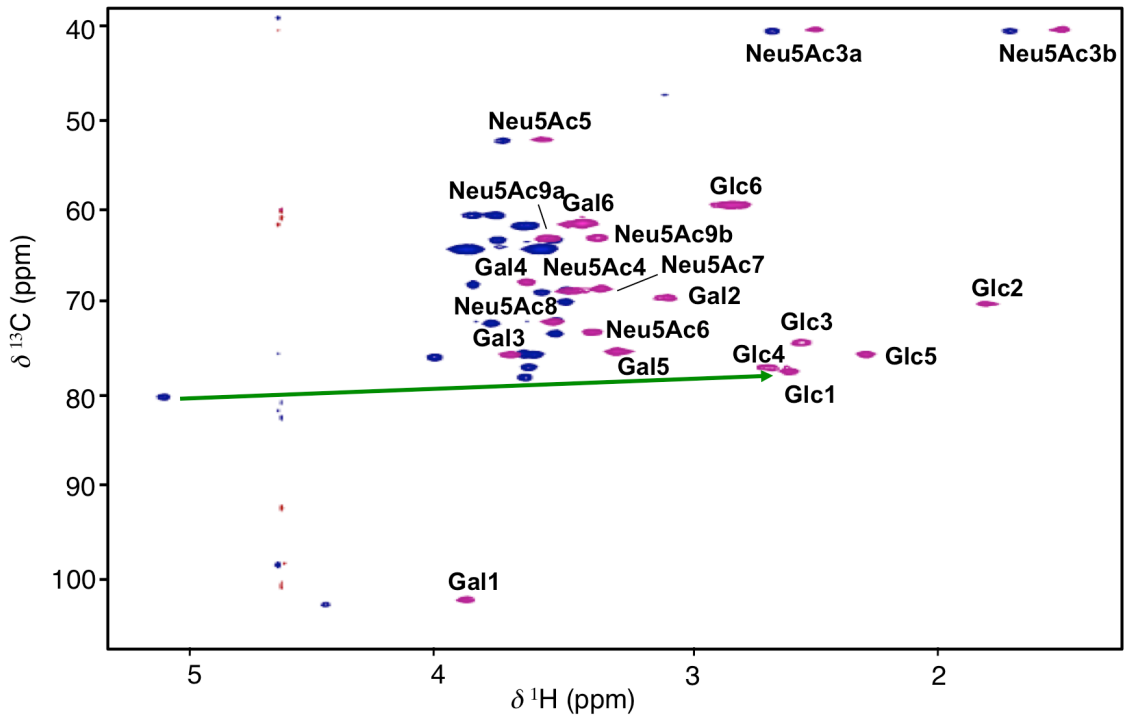


**Figure 2.1.** $^{1}H–^{13}C$ HSQC spectra of the GM3 trisaccharide tagged with $Tm^{3+}$ (magenta) and $La^{3+}$ (blue). Chemical shift differences of the anomeric CH groups are indicated by arrows.

**Table 2.1.** $^{1}H$ and $^{13}C$ chemical shifts of GM3 with the tag complexed with $La^{3+}$, $Tm^{3+}$, and $Tb^{3+}$.

| | $La^{3+}$ | | $Tm^{3+}$ | | $Tb^{3+}$ | |
|---|---|---|---|---|---|---|
| | $\delta^{1}H$/ppm | $\delta^{13}C$/ppm | $\delta^{1}H$/ppm | $\delta^{13}C$/ppm | $\delta^{1}H$/ppm | $\delta^{13}C$/ppm |
| Glc1 | 5.14 | 79.94 | 2.63 | 77.11 | 0.85 | 75.15 |
| 2 | 3.56 | 71.53 | 1.83 | 69.66 | 0.08 | 68.01 |
| 3 | 3.69 | 75.14 | 2.58 | 73.93 | 1.46 | 72.80 |
| 4 | 3.69 | 77.75 | 2.71 | 76.63 | 1.74 | 75.69 |
| 5 | 3.68 | 76.65 | 2.32 | 75.20 | 1.20 | 74.14 |
| 6 | 3.90 | 59.98 | 2.86 | 58.86 | 2.07 | 57.98 |
| | 3.80 | 59.97 | 2.82 | 58.86 | 1.96 | 57.98 |
| Gal 1 | 4.49 | 102.70 | 3.93 | 102.08 | 3.31 | 101.59 |
| 2 | 3.53 | 69.48 | 3.11 | 69.03 | 2.62 | 68.57 |
| 3 | 4.04 | 75.58 | 3.74 | 75.24 | 3.38 | 74.91 |
| 4 | 3.90 | 67.60 | 3.67 | 67.29 | 3.36 | 66.94 |
| 5 | 3.65 | 75.27 | 3.31 | 74.91 | 2.87 | 74.50 |
| 6 | 3.68 | 61.17 | 3.45 | 60.90 | 3.09 | 60.46 |
| | 3.68 | 61.16 | 3.45 | 60.90 | 2.98 | 60.47 |
| Neu5Ac 3 | 2.70 | 39.78 | 2.53 | 39.63 | 2.27 | 39.34 |
| 3 | 1.75 | 39.78 | 1.55 | 39.62 | 1.27 | 39.34 |
| 4 | 3.62 | 68.47 | 3.48 | 68.29 | 3.34 | 68.14 |
| 5 | 3.78 | 51.80 | 3.61 | 51.66 | 3.41 | 51.46 |
| 6 | 3.57 | 72.97 | 3.42 | 72.78 | 3.23 | 72.60 |
| 7 | 3.52 | 68.22 | 3.38 | 68.02 | 3.21 | 67.83 |
| 8 | 3.82 | 71.88 | 3.57 | 71.64 | 3.29 | 71.45 |
| 9 | 3.80 | 62.68 | 3.59 | 62.49 | 3.38 | 62.28 |
| | 3.57 | 62.69 | 3.40 | 62.48 | 3.20 | 62.28 |

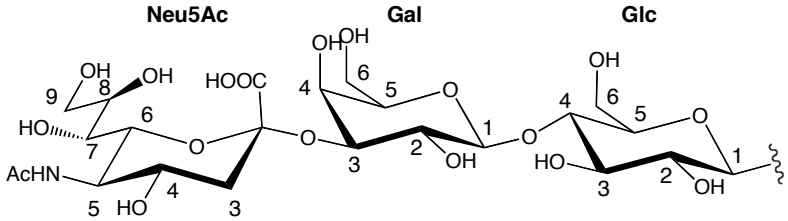

The PCSs were measured as the differences between the $^{1}H$ and $^{13}C$ chemical shifts of the compound chelated to the paramagnetic ion ($Tm^{3+}$ or $Tb^{3+}$) and those observed with the diamagnetic ion ($La^{3+}$) in their $^{1}H$–$^{13}C$ heteronuclear single–quantum coherence (HSQC) spectra (Figure 2.1 and Table 2.1). In this comparison, most of the CH groups exhibited PCS values sufficiently large for a quantitative conformational analysis, as summarized in Table 2.2. Significantly larger PCS values were observed for the H8 of Neu5Ac and its proximal atoms, suggesting a contribution of some bent conformations of this trisaccharide, which is consistent with a previously reported NMR study [10]. These experimentally determined PCS values were compared with those calculated from a conformational ensemble of the GM3 trisaccharide.

**Table 2.2.** Values of PCSs (ppm) derived from the $Tm^{3+}$ ion.

| | **Glc** | | **Gal** | | **Neu5Ac** | |
|---|---|---|---|---|---|---|
| | **$\Delta\delta^{13}C$** | **$\Delta\delta^{1}H$** | **$\Delta\delta^{13}C$** | **$\Delta\delta^{1}H$** | **$\Delta\delta^{13}C$** | **$\Delta\delta^{1}H$** |
| **1** | –2.83 | –2.51 | –0.62 | –0.56 | – | – |
| **2** | –1.87 | –1.73 | –0.45 | –0.42 | – | – |
| **3** | –1.22 | –1.12 | –0.34 | –0.30 | –0.16 | –0.17/–0.20 |
| **4** | –1.12 | –0.98 | –0.31 | –0.23 | –0.19 | –0.14 |
| **5** | –1.45 | –1.35 | –0.36 | –0.34 | –0.14 | –0.17 |
| **6** | –1.12 | –1.04/–0.98 | –0.27 | –0.23/–0.23 | –0.19 | –0.15 |
| **7** | – | – | – | – | –0.20 | –0.15 |
| **8** | – | – | – | – | –0.23 | –0.25 |
| **9** | – | – | – | – | –0.20 | –0.21/–0.17 |

### 2.2.2 Construction of conformational ensemble model

To generate atomic coordinates of the conformationally fluctuating trisaccaride, 10 MD simulations were performed in explicit water for 12 ns with the GLYCAM_06 force field

[12]. Consistent with the previously reported calculation, torsion angle pairs of this trisaccharide show high flexibility especially around the glycosidic linkage between the Neu5Ac and Gal residues (Figure. 2.2).

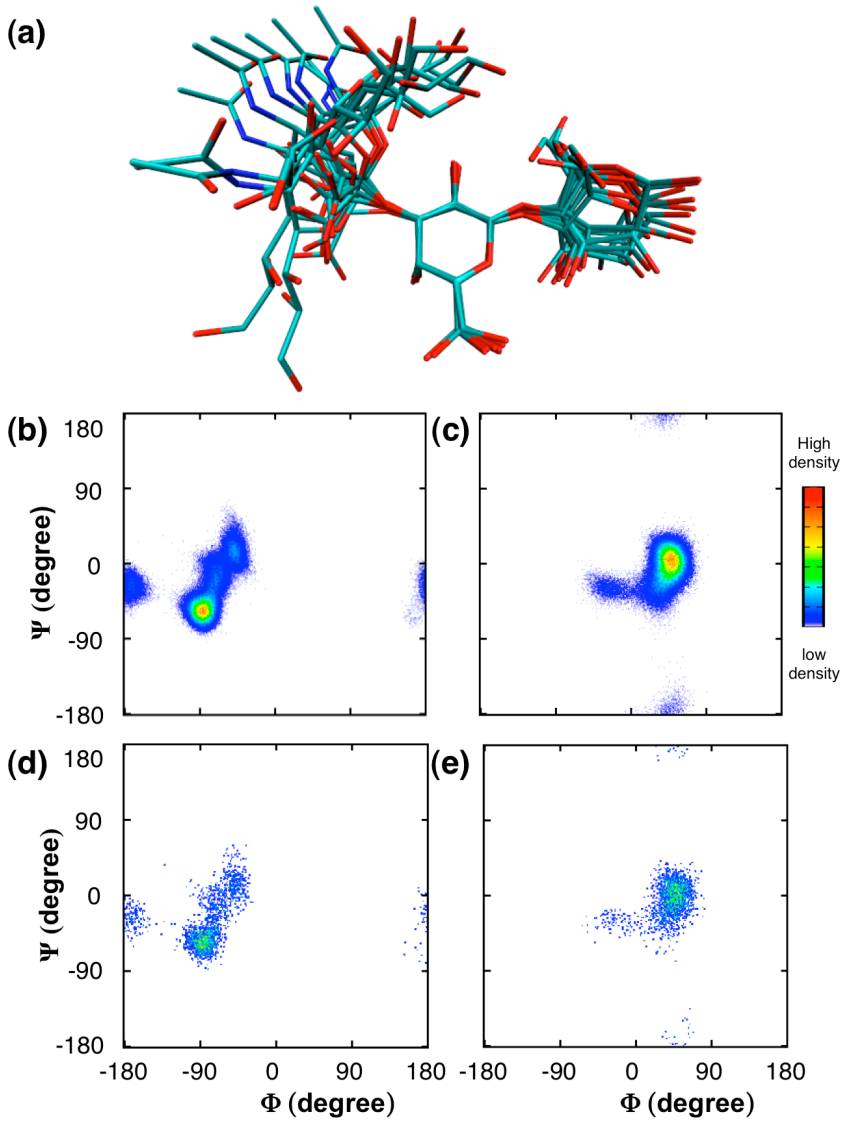


**Fig. 2.2** Conformational ensemble of the GM3 trisaccharide. (a) Snapshots of the GM3 trisaccharide from a simulated trajectory superimposed on the ring atoms of the Gal residue. All hydrogen atoms are omitted. Torsion angle density maps of MD trajectories of (b) the Neu5Ac–Gal linkage and (c) the Gal–Glc linkage. Scattered plots of torsion angles of (d) the Neu5Ac–Gal linkage and (e) the Gal–Glc linkage of the ensemble for PCS analysis. The NMR definitions of Φ and Ψ were used, namely, for the Neu5Ac–Gal linkage, Φ = C1–C2–O'3–C'3 and Ψ = C2–O'3–C'3–H'3 and the Gal–Glc linkage, Φ = H1–C1–O'4–C'4 and Ψ = C1–O'4–C'4–H'4.

All MD runs were combined after excluding the first 2 ns of trajectories. Subsequently, 2,000 trisaccharide conformers were extracted at equal intervals to create an ensemble model, which involved harmonic motions in a local minimum as well as transitions from one low–energy region to another in the energy landscape (Figure 2.2). The coordinate of the average position of the paramagnetic center with respect to the innermost Glc residue was defined from additional MD calculations of the tag moiety.

### 2.2.3 Comparison of experimental and theoretical PCS

A single $\Delta\chi$ tensor was determined for the conformational ensemble by inspection of the experimentally obtained PCSs with the assumption that every conformer contributes equally to the PCSs. The anisotropy values of the $\Delta\chi$ tensors $\Delta\chi_{ax}$ and $\Delta\chi_{rh}$, derived from the $Tm^{3+}$ ion for the ensemble, were estimated to be $8.1 \times 10^{-23}$ $m^3$ and $3.5 \times 10^{-23}$ $m^3$, respectively (Table 2.3). The results for the back–calculated PCSs were in excellent agreement with the experimental data: the *Q* value was 0.05 (Figure 2.3(a)). Similarly, a low *Q* (0.06) was obtained using $Tb^{3+}$ as a lanthanide probe (Figure 2.3(b)). Such low *Q* values could be obtained neither by employing most single conformers nor by using a combination of selected low–energy conformers (Table 2.3). Furthermore, a conformational ensemble derived from only one trajectory (12 ns), which do not include a low–populated conformational cluster in Gal–Glc linkage ($\Psi \sim -180°$), gave a compromised *Q* value (Figure 2.4).

**Table 2.3.** $Q$ and $\Delta\chi$ values of **1** complexed with $Tm^{3+}$ and $Tb^{3+}$.

| | $Tm^{3+}$ | $Tb^{3+}$ |
|---|---|---|
| [a]$Q$ | 0.05 | 0.06 |
| [b]$q_{ave}$ | 0.08 | 0.08 |
| [b]$q_{high}$ | 0.44 | 0.58 |
| [b]$q_{low}$ | 0.04 | 0.04 |
| $\chi_{ax}$ ($\times 10^{-23}$ $m^{-3}$) | 8.1 | 16.1 |
| $\chi_{rh}$($\times 10^{-23}$ $m^{-3}$) | 3.5 | 3.9 |
| [c]$\alpha$ | 28.1 | 26.6 |
| [c]$\beta$ | 20.1 | 16.3 |
| [c]$\gamma$ | –2.4 | –6.0 |
| [d]$Q_{selected}$ | 0.17 | 0.11 |

[a] $Q$ = rms($\Delta\delta_{calc}$ – $\Delta\delta_{obs}$)/rms($\Delta\delta_{obs}$). $\Delta\delta_{calc}$ is given by following equation; $\Delta\delta_{calc} = \sum_{i=1}^{N}(p_i \cdot 1/12\pi r_i^3 \cdot [\Delta\chi_{ax}(3\cos^2\vartheta_i - 1) + 2/3 \cdot \Delta\chi_{rh}(\sin^2\vartheta_i \cos 2\varphi_i)])$, where $p_i$ is populations of each structure (set to 0.0005), N is number of each conformers, and ($r_i$, $\vartheta_i$, $\varphi_i$) defines the position vector for conformer i of the nuclear in polar coordinates with respect to the metal center and principal axis of $\Delta\chi$ tensor.

[b] Average, highest and lowest value of $q_i$. $q_i$ = rms($\Delta\delta_{i,calc}$ – $\Delta\delta_{obs}$)/rms($\Delta\delta_{obs}$), where $\Delta\delta_{i,calc}$ is back–calculated PCSs for individual conformer as follows: $\Delta\delta_{i,calc} = 1/12\pi r_i^3 \cdot [\Delta\chi_{ax}(3\cos^2\vartheta_i - 1) + 2/3 \cdot \Delta\chi_{rh}(\sin^2\vartheta_i \cos 2\varphi_i)]$.

[c] The Euler angles for principal axis of $\Delta\chi$ tensor.

[d] $Q$ values are for a combination of selected conformers. The torsion angles for these structures were set to averaged values of torsion angles in each conformational cluster populated by more than 5%. Exact torsion values for Φ (Glc–Gal), Ψ (Glc–Gal), Φ (Gal–Neu5Ac), and Ψ (Gal–Neu5Ac) were 43, 1, −175, and −87; 43, 1, −89, and −89; 43, 1, −70, and −87 with a relative incidence estimated at 1:2:2, respectively.

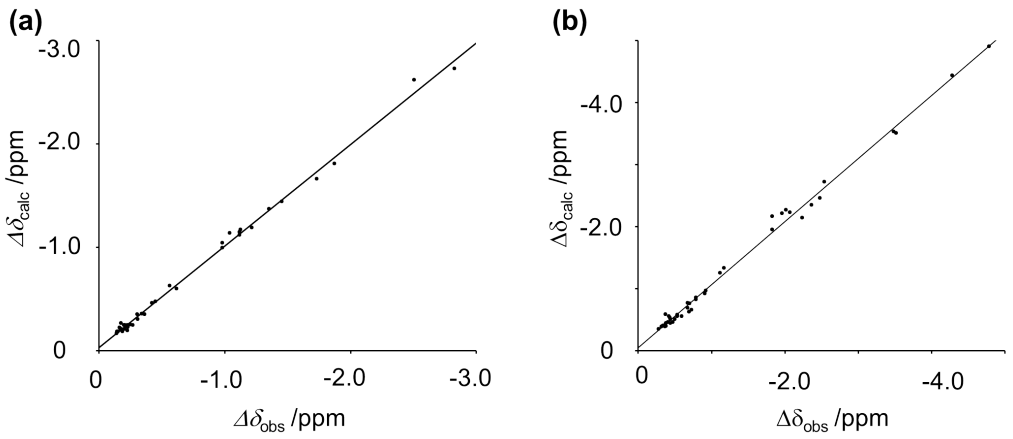


**Figure 2.3**. Correlations between the experimentally observed PCS values with (a) $Tm^{3+}$ and (b) $Tb^{3+}$ and back–calculated PCS values.

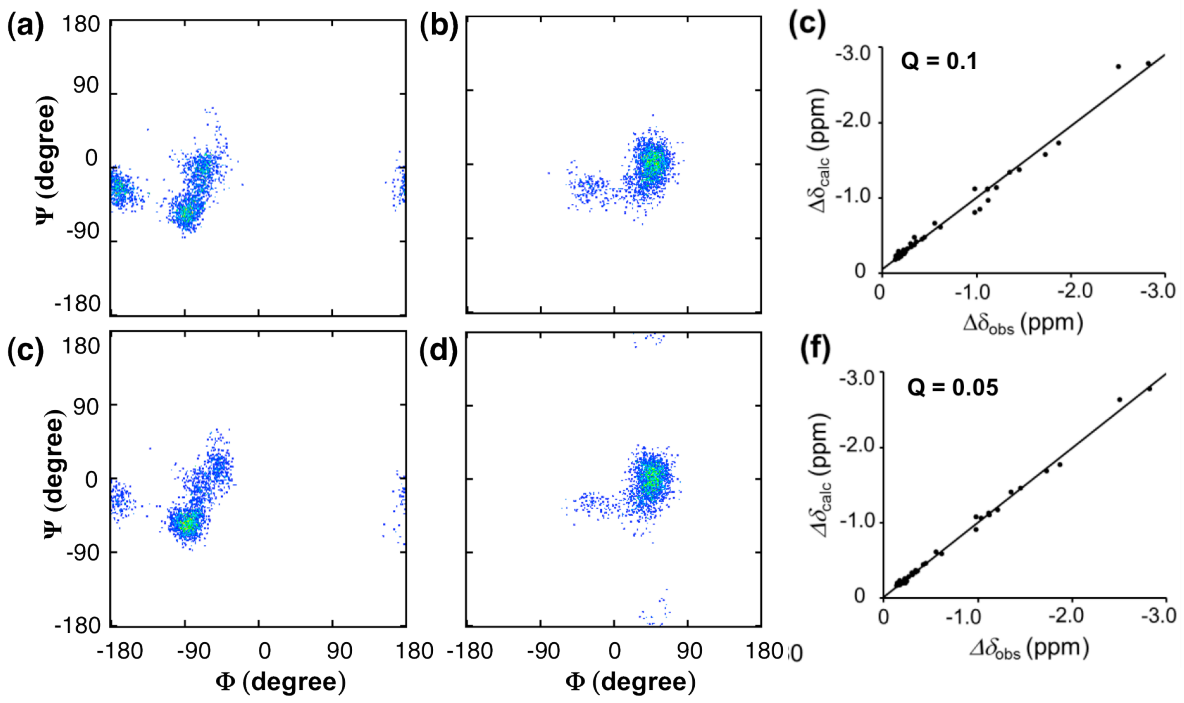


**Figure 2.4.** Influence of ensemble bias on the correlation between experimental and calculated PCS data. Scattaered plots of torsion angles of (a and d) the Neu5Ac–Gal linkage and (b and e) the Gal–Glc linkage of the ensembles and (c and f) the correlations between the experimentally observed PCS values with $Tm^{3+}$ and back–calculated PCS values. (a, b and c) 2,000 conformers from one trajectory (12 ns) gave Q value of 0.10. (d, e and f) 2,000 conformers from all 10 trajectory gave Q value of 0.05.

These results indicate that minor conformers significantly contribute to the observed PCS values. The minor "anti" conformations about the Gal–Glc linkage was barely detected in the MD simulation restrained by rotating frame Overhauser effect data that were obtained using $^{13}C$–enriched GM3 trisaccharide [10d]. These results demonstrated the utility of the lanthanide–assisted NMR method in conjunction with MD simulations in the evaluation of dynamic conformational ensembles of highly flexible oligosaccharides, considering their minor conformers in a systematic manner.

## 2.3 Conclusions

In summary, PCSs derived from the flexible GM3 trisaccharide was successfully acquired by the lanthanide–tagging method and interpreted the PCS data by inspecting a vast conformational ensemble of this flexible trisaccharide generated from MD simulations. The *Q* value difference between the conformational ensemble derived from only one trajectory (12 ns) without low–populated conformational cluster in Gal–Glc linkage ($\Psi \sim 180°$) and the conformational ensemble derived from 10 trajectories (120 ns) demonstrated the utility of the lanthanide–assisted NMR method in conjunction with MD simulations in the evaluation of dynamic conformational ensembles of highly flexible oligosaccharides, considering their minor conformers in a systematic manner.

## 2.4 Material and Experiments

### 2.4.1 General

Reagents and solvents were commercially available and used without any further purification unless otherwise noted. Column chromatography was performed using Silica Gel 60N purchased from Kanto Chemical Co., Inc., Wakosil 40C18 from Wako Pure Chemical Industries, Ltd., or Waters Sep–Pak C18. High–resolution MS measurements were performed

on a JEOL JMS–777V spectrometer (Akishima, Japan). The NMR spectra were recorded on a JEOL JNM ECA–600 spectrometer equipped with a 5–mm FG/HCN probe. TMS (in CDCl3) served as internal standard for the $^{1}H$– and $^{13}C$–NMR measurements.

### 2.4.2 MD Simulations of the sugar moiety of GM3

All–atom molecular dynamics simulations of the GM3 trisaccharide were employed using the Sander module of the Amber11 package [11] with the GLYCAM_06 force field [12]. To create the initial structure and topology file of the GM3 trisaccharide, the tLeap module of the AmberTools1.5 program [11] was used. TIP3P waters were added to the solvent layer to ensure a depth of at least 8 Å from any atom. Ten $Na^{+}$ ion and nine $Cl^{-}$ ion was added to neutralize the system. As a result, the simulation system contained 722 water molecules bringing the total number of atoms to 2,266. Before MD runs were performed, the entire system was energy minimized by 500 steps of steepest descent followed by 500 steps of conjugate gradient. The system was heated to 300 K with a 2–fs time step in the NPT ensemble [13] at 1 atm over 50 ps using isotropic position scaling. Production MD simulations were performed for 12 ns at 300 K with a 2–fs time step in the NPT ensemble. The initial velocities are randomized. Scaling of nonbonded 1–4 van der Waals and electrostatic interactions was not performed (i.e., SCEE = SCNB = 1.0). All bonds involving hydrogen atoms were constrained with the SHAKE algorithm [14], and long–range electrostatics were treated by the particle mesh Ewald method [15]. Snapshots were collected every 1 ps. Ten MD trajectories excluding the first 2 ns were combined into one. Analyses of the trajectories were performed using the PTRAJ module of the AmberTools1.5 program, and molecular graphics images were produced using VMD [16].

**Definition of the paramagnetic center:**

MD simulations of the lanthanum–chelating tag attached to a terminal glucose residue to consider the motion of the tag moiety were performed. The initial structures were built by modifying a previously reported crystal structure of $[Fe(1,2–(N(CH_2COO)_2)_2C_6H_4 \cdot H_2O]^-$, and their torsion angles for the rotatable C–C bond between benzene and the amide group were set to 0° or 180°. The Antechamber program [17], in combination with the general Amber force field (GAFF) [18], was used to generate parameters for the glucose–attached tag without a lanthanum ion. The charge of the glucose and tag component were assigned by the AM1–BCC method [19]. For the $La^{3+}$ ion, previously reported parameters were used [20]. The topology file for the molecule with the $La^{3+}$ ion was created with the tLeap module. TIP3P waters were added to the solvent layer to ensure a depth of at least 8 Å from any atom. Ten $Na^+$ ions and nine $Cl^-$ ions were added to neutralize the system. The distance between the $La^{3+}$ ion and the carboxyl oxygen or diamine nitrogen atoms of the tag was restrained to be 2.3 or 2.5 Å, respectively. Before MD runs were performed, the entire system was energy minimized by 500 steps of steepest descent followed by 500 steps of conjugate gradient and then heated to 300 K with a 2–fs time step in the NPT ensemble at 1 atm over 50 ps. Production MD simulations were performed for 30 ns at 300 K with a 2–fs time step in the NPT ensemble. The simulations were carried out twice for each initial structure. All bonds involving hydrogen atoms were constrained by the SHAKE algorithm and long–range electrostatics were treated by the particle mesh Ewald method. Snapshots were collected every 1 ps. By averaging the coordinate of the $La^{3+}$ ion over the trajectories except the first 5 ns, the position of the paramagnetic center relative to the six–membered ring of glucose was defined.

**Tensor determination:**

Two thousand conformers were extracted from the combined trajectory of the GM3

trisaccharide every 50 ps, and the averaged paramagnetic center was added by aligning each glucose ring. The χ tensor for the ensembles incorporating either the $Tm^{3+}$ ion or $Tb^{3+}$ ion was determined by a modified version of Mspin [21]. Every conformer was estimated to contribute equally to the PCSs.

### 2.4.3 Preparation of the tagged GM3 trisaccahride

**Preparation of metal chelating unit 2:**

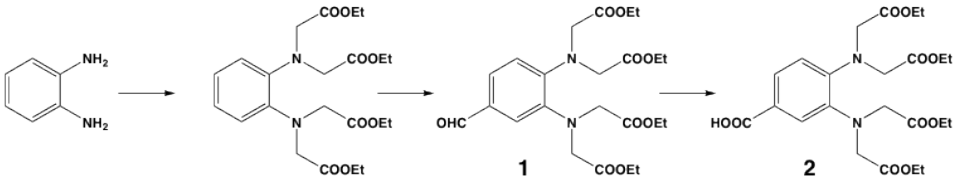


The precursor **1** was synthesized from *o*–phenylenediamine in 2 steps [22] $NaH_2PO_4$ (2.6 g, 21.8 mmol) and $NaClO_2$ (2.4 g, 32.8 mmol) were dissolved in $H_2O$ (20 mL) and then transferred to the solution of **1** (1.3 g, 2.7 mmol) and 2–methyl–2–butene (2.9 mL, 27.2 mmol) in *tert*–butyl alcohol (20 mL). The mixture was stirred at RT for 7 h, and then concentrated and neutralized with HCl (1 M) aqueous. This mixture was extracted with EtOAc, dried with $Na_2SO_4$ and concentrated. The residue was purified on a silica gel column with EtOAc/Hexane (1:1) to give **2** (1 g, 74%). $^1$H–NMR ($CDCl_3$, 300 K): δ = 7.80 (d, *J* = 1.38Hz, 1H, Ar*H*), 7.70 (dd, *J* = 8.3, 1.4 Hz, 1H, Ar*H*), 7.02 (d, *J* = 8.9 Hz, 1H, Ar*H*), 4.39 (s, 4H, N($CH_2$)$_2$), 4.26 (s, 4H, N($CH_2$)$_2$), 4.11(m, 8H, COO$CH_2$), 1.20 (dd, *J* = 14.1, 7.13Hz, 12H, $CH_2CH_3$); $^{13}$C–NMR ($CDCl_3$, 300 K): δ = 171.9, 171.0, 147.5, 141.0, 126.0, 124.1, 126.0, 120.5, 61.0, 52.4, 14.1; HRMS (FAB): Calcd for $C_{23}H_{33}N_2O_{10}$ [M+$H^+$]: 497.2135; Found: 497.2130.

**Preparation of azide 4:**

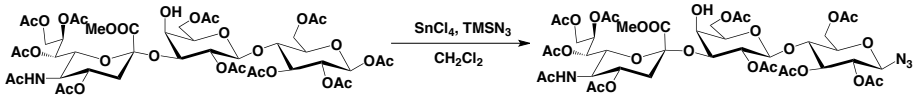


**3** **4**

Trimethylsiylazide (179 μL, 1.36 mmol) and $SnCl_4$ (83.75 μL, 0.715 mmol) was added at 0 °C to a solution of compound **3** (371 mg, 0.335 mmol) in $CH_2Cl_2$ (5mL). The mixture was stirred at RT for 12 h. Then the reaction mixture was diluted with $CHCl_3$, washed with saturated aqueous $NaHCO_3$, $H_2O$, dried with $Na_2SO_4$ and concentrated. The residue was purified by column chromatography on silica gel ($CHCl_3$/MeOH 20:1) to give **4** (320 mg, 88%). $^1$H–NMR ($CDCl_3$, 300 K): δ = 5.52 (m, 1H, Neu8), 5.38 (dd, *J* = 9.65, 2.86 Hz, 1H, Neu7), 5.18 (t, *J* = 9.37 Hz, 1H, Glu3), 5.03 (d, *J* = 10.4 Hz, 1H, N*H*), 4.94–4.81 (m, 4H, Gal2, 4, Neu4, Glu2), 4.67 (d, *J* = 7.60 Hz, 1H, Gal1), 4.62 (d, *J* = 8.26 Hz, 1H, Glu1), 4.51 (dd, *J* = 10.3, 3.44 Hz, 1H, Gal3), 4.47 (dd, *J* = 11.7, 2.04 Hz, 1H, Gal6a), 4.41 (dd, *J* = 12.4, 2.70 Hz, 1H, Gal6b), 4.18 (dd, *J* = 11.7, 5.56 Hz, 1H, Glu6a), 4.00 (m, 4H, Glu6b, Neu5, 9), 3.89 (t, *J* = 9.65 Hz, 1H, Glu4), 3.83 (4H, COOMe, Gal5), 3.69 (m, 1H, Glu5), 3.61 (dd, *J* = 11.0, 2.74 Hz, Neu6), 2.56 (dd, *J* = 12.7, 4.48 Hz, 1H, Neu3a), 2.23–1.99 (m, 33H, OAc), 1.84 (s. 3H, NHAc), 1.66 (t, *J* = 12.4 Hz, 1H, Neu3b); $^{13}$C–NMR ($CDCl_3$, 300 K): δ = 171.7 171.3, 171.0, 170.2, 169.4, 168.5, 101.2, 97.1, 87.8, 76.1, 75.0, 74.9, 73.3, 72.2, 71.4, 71.2, 70.6, 70.0, 69.9, 69.4, 67.8, 67.3, 67.0, 62.3, 62.1, 61.5, 53.3, 49.3, 37.5, 23.3, 21.6, 21.0, 20.7; HRMS (FAB): Calcd for $C_{44}H_{61}N_4O_{28}$ [M+H$^+$]:1093.3472; Found:1093.3483.

**Preparation of amine 5:**

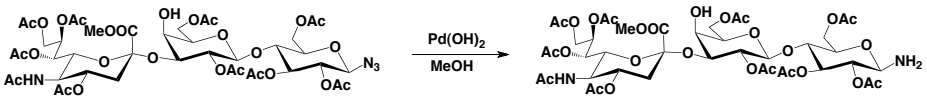


**4** **5**

Compound **4** (270mg, 0.247mmol) was dissolved in MeOH (5 mL), to this solution was added Pd/C (4.8 mg). The mixture was stirred in hydrogen atmosphere at RT for 12 h. The reaction mixture was filtered through celite and concentrated, then purified by column chromatography on silica gel ($CHCl_3$/MeOH 20:1) to give **5** (200 mg, 76%). $^1$H–NMR ($CDCl_3$, 300 K): δ = 5.51 (m, 1H, Neu8), 5.38 (dd, *J* = 9.64, 2.70 Hz, 1H, Neu7), 5.19 (t, *J* = 9.31 Hz, 1H, Glu3), 5.03 (d, *J* = 10.4 Hz, 1H, N*H*), 4.90 (m, 3H, Gal4, Neu4, Gal2), 4.71 (t, *J* = 9.57 Hz, 1H, Glu2), 4.62 (d, *J* = 8.23 Hz, 1H, Gal1), 4.50 (dd, *J* = 9.67, 3.35 Hz, 1H, Gal3), 4.40 (m, 2H, Gal6), 4.14 (m, 2H, Glu1, 6a), 3.99 (m, 4H, Glu6b, Neu5, 9), 3.83 (br, 4H, Gal5, COOMe), 3.78 (t, *J* = 9.57 Hz, 1H, Glu4), 3.60 (m, 2H, Neu6, Glu5), 2.54 (dd, *J* = 12.7, 4.45 Hz, 1H, Neu3a), 1.99–2.23 (m, 33H, OAc), 1.85 (s. 3H, NHAc), 1.66 (t, *J* = 12.3 Hz, 1H, Neu3b); $^{13}$C–NMR ($CDCl_3$, 300 K): δ = 171.4, 171.2, 171.1, 170.9, 170.2, 168.4 101.0, 97.5, 84.6, 76.6, 73.7, 73.5, 72.6, 72.1, 71.6, 70.5, 70.0, 69.4, 67.8, 67.4, 67.0, 62.6, 62.3, 61.7, 53.3, 49.1, 31.3, 23.3, 21.6, 21.0, 20.7. EA: Calcd for $C_{44}H_{62}N_2O_{28}$•$2H_2O$: C, 47.91; H, 6.03; N, 2.54. Found: C, 48.02; H, 5.89; N, 2.25.

**Preparation of compound 6:**

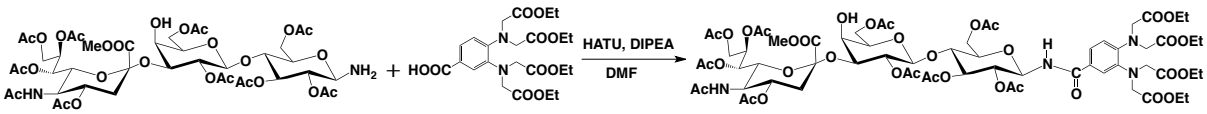


**5** **2** **6**

Compound **2** (100 mg, 0.20 mmol), DIPEA (0.35 mL, 2 mmol) and HATU (77.1mg, 0.20 mmol) was dissolved in DMF (5 mL) and the mixture was stirred at RT for 10 min. Subsequently, the mixture was transferred to a solution of compound **5** (180 mg, 0.169 mmol)

and DIPEA (17.3 μL, 0.1 mmol) in DMF (1 mL) and this solution was stirredat RT for 12 h. Reaction mixture extracted with EtOAc, washed with $H_2O$, dried with $Na_2SO_4$ and concentrated.The residue was purified on a silica gel column with $CHCl_3$/MeOH (25:1) to give **6** (36 mg, 25%). $^1$H–NMR ($CDCl_3$, 300 K): δ = 7.51 (dd, *J* = 1.3 Hz, 1H, Ar*H*), 7.25 (1H, Ar*H*), 7.00 (dd, *J* = 8.2 Hz, 1H, Ar*H*), 6.82 (d, *J* = 8.85 Hz, 1H, N*H*CO), 5.47 (m, 1H, Neu8), 5.40 (dd, *J* = 9.44, 2.55 Hz, 1H, Neu7), 5.33 (m, 2H, Glu1, 3), 5.07 (d, *J* = 9.78 Hz, 1H, N*H*), 4.91 (m, 4H, Glu2, Gal2, 4,Neu4), 4.61 (d, *J* = 7.71 Hz, Gal1), 4.50 (dd, *J* = 10.3, 3.47 Hz, Gal3), 4.45–4.15 (m, 11H, N(C$H_2$)$_2$, Gal6, Glu6a), 4.1 (m, 8H, N(C$H_2$)$_2$), 4.0 (m, Neu5, 9, Glu6b), 3.85 (m, 6H, COOMe, Gal5, Glu4, 5), 3.62 (dd, *J* = 11.0, 2.75 Hz, 1H, Neu6), 2.56 (dd, *J* = 13.1, 4.90 Hz, 1H, Neu3a), 2.24–1.97 (m, 33H, OAc), 1.8 (s, 3H, NHAc), 1.66 (t, *J* = 12.3 Hz, 1H, Neu3b), 1.2 (m, 12H, $CH_2CH_3$); $^{13}$C–NMR ($CDCl_3$, 300 K): δ = 172.6, 171.4, 171.2, 171.0, 168.5, 167.2, 163.0, 145.7, 141.7, 127.6, 122.0, 121.6, 120.7, 101.0, 78.9, 76.1, 74.6, 72.6, 72.1, 71.5, 70.5, 70.0, 69.4, 68.0, 67.8, 67.4, 66.8, 62.1, 61.8, 60.8, 52.1, 53.3, 53.1, 49.2, 53.3, 37.5, 23.2, 21.0, 21.6, 20.8, 14.2, HRMS (FAB): Calcd for $C_{67}H_{93}N_4O_{37}$ [M+H$^+$]:1545.5519; Found: 1545.5511.

**Preparation of modified trisaccharide 7:**

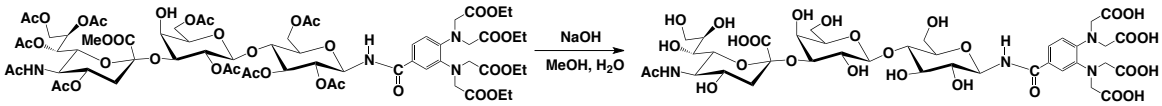


**6** **7**

Compound **6** (60 mg) was dissolved in MeOH and small aliquots ofNaOH (1 M) aqueous solution were added until the reaction was complete (TLC). The reaction mixture was purified by ODS column to give **7** (32 mg, 83%). $^1$H–NMR (600 MHz, $D_2O$, 300 K): δ =7.32 (s, 1H, Ar*H*), 7.29 (d, *J* = 8.27 Hz, 1H, Ar*H*), 6.81 (d, *J* = 8.17 Hz, 1H, Ar*H*), 5.11 (d, *J* = 9.59 Hz, Glu1), 4.49 (d, *J* = 7.89 Hz, Gal1), 4.13 (m, 4H, N(C$H_2$)$_2$), 4.05 (dd, *J* = 9.7, 6.8 Hz,

1H, Gal3), 3.93–3.86 (m, 6H, N(C$H_2$)$_2$, Gal4, Glu6a), 3.82–3.76 (m, 4H, Neu5, 8, 9a, Glu6b), 3.70–3.62 (m, 7H, Gal5, 6, Glu3, 4, 5, Neu4), 3.56–3.52 (m, 5H, Gal2, Glu2, Neu6, 7, 9b), 2.68 (dd, $J$ = 12.4, 7.88 Hz, Neu3a), 1.95 (s, 3H, NHAc), 1.72 (t, $J$ = 12.1 Hz, 1H, Neu3b); $^{13}$C–NMR (150 MHz, $D_2O$, 300 K): δ = 178.8, 175.3, 174.2, 171.7, 146.2, 140.2, 125.4, 123.1, 121.1, 102.6, 100.1, 80.1, 77.8, 76.6, 75.6, 75.3, 75.2, 73.0, 71.9, 71.6, 69.4, 68.5, 68.2, 67.6, 62.6, 61.0, 59.9, 54.6, 54.1, 51.6, 39.5, 21.8.

### 2.4.4. PCS observation of the tagged sugar

Compound **7** (2mg) was dissolved in $D_2O$ (0.6 ml) and pH was increased to 8.0 by adding NaOD solution. This solution was titrated with $D_2O$ solution of $MCl_3$ (250mM; M = $La^{3+}$, $Tm^{3+}$ or $Tb^{3+}$) for NMR measurements. For PCS observation, $^1$H–$^{13}$C HSQC spectra were recorded at 300 K with 512 ($t_1$) and 1024 ($t_2$) complex points. NMR spectra were processed and analyzed with the programs NMRPipe [23] and Sparky [24].

## References:


1. **(a)** M. R. Wormald, A. J. Petrescu, Y. L. Pao, A. Glithero, T. Elliott and R. A. Dwek, Conformational studies of oligosaccharides and glycopeptides: complementarity of NMR, X–ray crystallography, and molecular modelling. *Chem. Rev.,*102 (**2002**) 371–386. **(b)** Y. Kamiya, M. Yagi–Utsumi, H. Yagi and K. Kato, Structural and molecular basis of carbohydrate–protein interaction systems as potential therapeutic targets. *Curr. Pharm. Des*., 17 (**2011**) 1672–1684. **(c)** J. Hölmgren, I. Lönnroth, J. Månsson, L. Svennerholm, Interaction of cholera toxin and membrane GM1 ganglioside of small intestine. *Proc Natl Acad Sci USA* 72 (**1975**) 2520–2524. **(d)** U. Neu, K. Woellner, G. Gauglitz, T. Stehle, Structural basis of GM1 ganglioside recognition by simian virus

40. *Proc Natl Acad Sci USA* 105 (**2008**) 5219–5224. **(e)** J. Kopitz, C. von Reitzenstein, M. Burchert, M. Cantz, H. J. Gabius, Galectin–1 is a major receptor for ganglioside GM1, a product of the growth–controlling activity of a cell surface ganglioside sialidase, on human neuroblastoma cells in culture. *J Biol Chem* 273 (**1998**) 11205–11211.

2. **(a)** Y. Kamiya, T. Satoh, K. Kato, Molecular and structural basis for N–glycan dependent determination of glycoprotein fates in cells, *Biochim. Biophys. Acta,* 1820 (**2012**) 1327–1337. (b) N. Yuki, Carbohydrate mimicry: a new paradigm of autoimmune diseases. *Curr Opin Immunol* 17 (**2005**) 577–582.
3. C. A. Stortz, G. P. Johnson, A. D. French, G. I. Csonka, Comparison of different force fields for the study of disaccharides, *Carbohydr Res* 344 (**2009**) 2217–2228.
4. **(a)** I. Bertini, C. Luchinat, G. Parigi, Magnetic susceptibility in paramagnetic NMR, P*rog. Nucl. Magn. Reson. Spectrosc.* 40 (**2002**) 249–273. **(b)** P. H. Keizers and M. Ubbink, Paramagnetic tagging for protein structure and dynamics analysis, *Prog. Nucl. Magn. Reson. Spectrosc.,* 58 (**2011**) 88–96. **(c)** G. Otting, Protein NMR using paramagnetic ions, An*nu. Rev. Biophys.,* 39 (**2010**) 387–405.
5. I. Bertini, A. Donaire, B. Jimenez, C. Luchinat, G. Parigi, M. Piccioli and L. Poggi, Paramagnetism–based versus classical constraints: an analysis of the solution structure of Ca Ln calbindin D9k, *J. Biomol. NMR*, 21 (**2001**) 85–98.
6. **(a)** C. Ma, S. J. Opella, Lanthanide ions bind specifically to an added ‘‘EF–hand’’ and orient a membrane protein in micelles for solution NMR spectroscopy, *J Magn Reson* 146 (**2000**) 381–384. **(b)** J. Wöhnert, K. J. Franz, M. Nitz, B. Imperiali, H. Schwalbe, Protein alignment by a coexpressed lanthanide–binding tag for the measurement of residual dipolar couplings. *J Am Chem Soc* 125 (**2003**) 13338–13339.

7. **(a)** A. Dvoretsky, V. Gaponenko, P. R. Rosevear, Derivation of structural restraints using a thiol–reactive chelator. *FEBS Lett* 528 (**2002**) 189–192. **(b)** X. C. Su, T. Huber, N. E. Dixon, G. Otting, Site–specific labelling of proteins with a lanthanide–binding tag. *Chem Bio Chem* 7 (**2006**) 1469–1474. **(c)** X. C. Su, K. McAndrew, T. Huber, G. Otting, Lanthanide–binding peptides for NMR measurements of residual dipolar couplings and paramagnetic effects from multiple angles. *J Am Chem Soc* 130 (**2008**) 1681–1687.

8. **(a)** T. Saio, M. Yokochi, H. Kumeta, F. Inagaki, PCS–based structure determination of protein–protein complexes, *J Biomol NMR* 46 (**2010**) 271–280. **(b)** G. Pintacuda, A. Y. Park, M. A. Keniry, N. E. Dixon, and G. Otting, Lanthanide labeling offers fast NMR approach to 3D structure determinations of protein–protein complexes, *J. Am. Chem Soc.* 128 (**2006**) 3696–3702.

9. **(a)** S. Yamamoto, T. Yamaguchi, M. Erdélyi, C. Griesinger and K. Kato, Paramagnetic Lanthanide Tagging for NMR conformational analyses of N–linked oligosaccharides, *Chem.–Eur. J.,* 17 (**2011**) 9280–9282. **(b)** M. Erdélyi, E. d'Auvergne, A. Navarro–Vázquez, A. Leonov and C. Griesinger, Dynamics of the glycosidic bond: conformational space of lactose, *Chem.–Eur. J.,* 17 (**2011**) 9368–9376. **(c)** A. Mallagaray, A. Canales, G. Domínguez, J. Jiménez–Barbero and J. Pérez–Castells, A rigid lanthanide binding tag for NMR structural analysis of carbohydrates**,** *Chem. Commun.,* 47 (**2011**) 7179–7181.

10. **(a)** H. C. Siebert, G. Reuter, R. Schauer, C. W. von der Lieth and J. Dabrowski, Solution conformations of GM3 gangliosides containing different sialic acid residues as revealed by NOE–based distance mapping, molecular mechanics, and molecular dynamics calculations, *Biochemistry*, 31 (**1992**) 6962–6971. **(b)** Y. Aubin, Y. Ito, J. C. Paulson and J. H. Prestegard, Structure and dynamics of the sialic acid moiety of GM3–

ganglioside at the surface of a magnetically oriented membrane, *Biochemistry*, 32 (**1993**) 13405–13413. **(c)** G. R. Kiddle and S. W. Homans, Residual dipolar couplings as new conformational restraints in isotropically $^{13}$C–enriched oligosaccharides, *FEBS Lett.*, 436 (**1998**) 128–130. **(d)** M. J. Milton, R. Harris, M. A. Probert, R. A. Field and S. W. Homans, New conformational constraints in isotopically ($^{13}$C) enriched oligosaccharides, *Glycobiology*, 8 (**1998**) 147–153. **(e)** M. L. DeMarco and R. J. Woods, Atomic–resolution conformational analysis of the GM3 ganglioside in a lipid bilayer and its implications for ganglioside–protein recognition at membrane surface, *Glycobiology*, 19 (**2009**) 344–355.

11. D. A. Case, T. A. Darden, T. E. Cheatham, C. L. Simmerling, J. Wang, R. E. Duke, R. Luo, R. C. Walker, W. Zhang, K. M. Merz, B. P. Roberts, B. Wang, S. Hayik, A. Roitberg, G. Seabra, I. Kolossvai, K. F. Wong, F. Paesani, J. Vanicek, J. Liu, X. Wu, S. R. Brozell, T. Steinbrecher, H. Gohlke, Q. Cai, X. Ye, J. Wang, M.–J. Hsieh, G. Cui, D. R. Roe, D. H. Mathews, M. G. Seetin, C. Sagui, V. Babin, T. Luchko, S. Gusarov, A. Kovalenko and P. A. Kollman, Amber11, (**2010**) University of California, San Francisco.
12. K. N. Kirschner, A. B. Yongye, S. M. Tschampel, J. González–Outeiriño, C. R. Daniels, B. L. Foley and R. J. Woods, GLYCAM06: A generalizable biomolecular force field. carbohydrates, *J. Comput. Chem.,* 29 (**2008**) 622–655.
13. H. J. C. Berendsen, J. P. M. Postma, W. F. van. Gunsteren, A. DiNola and J. R. Haak, Molecular dynamics with coupling to an external bath, *J. Chem. Phys.*, 81 (**1984**) 3684–3691.
14. J. P. Ryckaert, G. Ciccotti and H. J. C. Berendsen, Numerical integration of the cartesian equations of motion of a system with constraints: molecular dynamics of n–alkanes, *J. Comput. Phys.*, 23 (**1977**) 327–341.

15. T. Darden, D. York and L. Pedersen, Particle mesh Ewald: An W log(N) method for Ewald sums in large systems, *J. Chem. Phys.,* 98 (**1933**) 10089–10093.

16. W. Humphrey, A. Dalke and K. Schulten, VMD – visual molecular dynamics, *J. Molec. Graphics,* 14 (**1996**) 33–38.

17. J. Wang, W. Wang, P. A. Kollman and D. A. Case, Automatic atom type and bond type perception in molecular mechanical calculations, *J. Mol. Graph. Model.*, 25 (**2006**) 247–260.

18. J. Wang, R. M. Wolf, J. W. Caldwell, P. A. Kollman and D. A. Case, Development and testing of a general amber force field, *J. Comput. Chem.,* 25 (**2004**) 1157–1174.

19. A. Jakalian, B. L. Bush, D. B. Jack and C. I. Bayly, Fast, efficient generation of high–quality atomic charges. AM1–BCC model: I. Method, *J. Comput. Chem.*, 21 (**2000**) 132–146.

20. M. Baaden, F. Berny, C. Madic and G. Wipff, $M^{3+}$ lanthanide cation solvation by acetonitrile: the role of cation size, counterions, and polarization effects investigated by molecular dynamics and quantum mechanical simulations, *J. Phys. Chem. A*, 104 (**2000**) 7659–7671.

21. V. M. Sánchez–Pedregal, R. Santamaría–Fernández and A. Navarro–Vázquez, Residual dipolar couplings of freely rotating groups in small molecules. Stereochemical assignment and side–chain conformation of 8–phenylmenthol. *Org. Lett.,* 11 (**2009**) 1471–1474.

22. J. Wang and X. Qian, A series of polyamide receptor based PET fluorescent sensor molecules: positively cooperative $Hg^{2+}$ ion binding with high sensitivity, *Org. Lett.,* 8 (**2006**) 3721–3724.

23. F. Delaglio, S. Grzesiek, G. W. Vuister, G. Zhu, J. Pfeifer and A. Bax, NMRPipe: A multidimensional spectral processing system based on UNIX pipes, *J. Biomol. NMR*, 1995, 6, 277–293.

24. T. D. Goddard and D. G. Kneller, SPARKY 3, University of California, San Francisco.

**Supporting information**

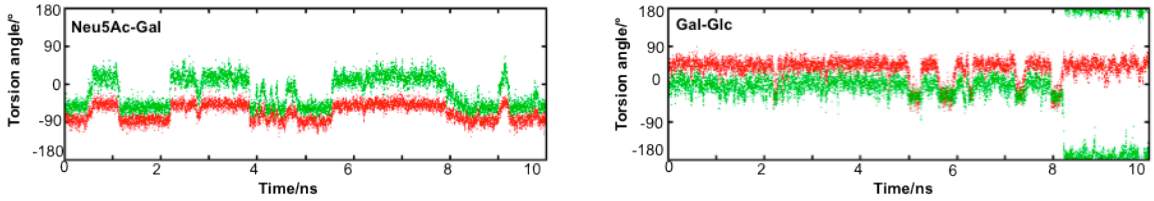


The figure shows the time evolution of the torsion angles of the glycosidic linkage in GM3 trisaccharide obtained from an MD trajectory, which contains the minor GM3 conformers with the angle Ψ of the Gal–Glc glycosidic linkage at ± 180° shown in the torsion angle map of GM3 trisaccharide (See Fig 2.2). Green lines represent the torsion angle Ψ, red lines represent the torsion angle Φ.

These data were choosen from 10 trajectories of the 12–ns simulation results, excluding the first 2–ns part.

# Chapter 3: Application of paramagnetic NMR–validated molecular dynamics simulation for characterization of the conformational dynamics of branched GM2 and GM1 oligosaccharides

This chapter is partially adapted and modified from Ying Zhang, Sayoko Yamamoto, Takumi Yamaguchi and Koichi Kato, Application of Paramagnetic NMR–Validated Molecular Dynamics Simulation to the Analysis of a Conformational Ensemble of a Branched Oligosaccharide, Molecules 2012, 17, 6658–6671.

## 3.1 Introduction

Another unique structural feature of oligosaccharides in addition to the inherent flexibility of glycosidic linkages is their branching with multiple modes of linkages in contrast to nucleic acids, and proteins. The branching of oligosaccharides is also important for them functioning in living system. One of the typical examples is high–mannose–type oligosaccharides such as triantennary Glc3Man9GlcNAc2 tetradecasaccharide (Manα1–2Manα1–6(Manα1–3)Manα1–6(Glcα1–2Glcα1–3Galα1–3Manα1–2Manα1–2Manα1–3) Manβ 1–4GlcNAcβ1–4GlcNAc) which is a common precursor of *N*–linked oligosaccharides on glycoproteins [2]. The distinct glycotopes displayed on the triantennary high–mannose–type oligosaccharides are recognized by intracellular lectins functioning as molecular chaperones and cargo receptors or by those involved in protein degradation system, and thus determine the fates of the glycoproteins in cells [3]. Although the high–mannose–type glycans contain the αManα–(1-2)–αMan disaccharide on each branch, the intracellular lectins have selectively bind to the specific branch [4]. This indicates that the 3D structure of each branch of high–mannose–type glycan determines the binding specificity of lectins and also implied the importance of analyzing the dynamic 3D structure of branched oligosaccharides.

In Chapter 2, a systematic method by the combination of PCS and MD simulation has been developed. Large–scale MD simulations in conjunction with lanthanide–assisted NMR spectroscopy enabled the atomic description of a dynamic ensemble of the conformations of a linear trisaccharide of ganglioside GM3 (αNeu5Ac–(2–3)–βGal–(1–4)–βGlc) in solution [5]. In this approach, a metal–chelating tag was covalently attached to the reducing end of the trisaccharide for observing PCSs, which depend on the relative positions of the individual atoms with respect to the lanthanide ion coordinated at the tag. The observed PCS values are compared with those back–calculated from the MD–derived conformational ensemble of the trisaccharide to validate the simulation result. This method was useful in evaluating the

dynamic conformational ensembles of oligosaccharides, considering minor conformers that are barely detected by other experimental techniques.

Herein, this approach was attempted to apply to the conformational characterization of branched oligosaccharides by using GM2 tetrasaccharide (βGalNAc–(1–4)–[αNeu5Ac–(2–3)]–βGal–(1–4)–βGlc) and GM1 pentasaccharide (βGal–(1–4)–βGalNAc–(1–4)–[αNeu5Ac–(2–3)]–βGal–(1–4)–βGlc), which possess an additional branch in comparison with the GM3 trisaccharide. It is reported that these branced gangliosides are also involved in numerous biological activities. Conformational dynamics analyses of the branched oligosaccharides are very crucial to understand the underlying mechanism of their functions. By comparing the experimental data and simulation results of the GM1, GM2 and GM3 glycans, the dynamic conformational change triggered by the branching structure was found.

## 3.2 Results and Discussion

### 3.2.1 Analyses of the conformational dynamics of GM2 tetrasaccharide

**3D structural ensemble construction:**

The initial structure for the simulation of GM2 tetrasaccharide was determined on the basis of preliminary MD calculations, in which the glycosidic torsion angles Φ and Ψ were 39.8° and –43.6° for Gal–Glc, 42.1° and 16.9° for GalNAc–Gal, and −175.2° and −25.6° for Neu5Ac–Gal linkages. Based on this initial state, all–atom MD simulations with the GLYCAM_06 force field [6] were employed to capture the conformational dynamics of the sugar moiety of GM2. Ten MD simulations were performed in explicit water for 12 ns at 300 K to generate the atomic coordinates of the tetrasaccharide. All MD runs were combined after excluding the first 2 ns of trajectories. Subsequently, 2,000 GM2 tetrasaccharide conformers were extracted at equal intervals to create an ensemble model. Torsion angles of the glycosidic linkages of the conformational ensemble were monitored (Figure 3.1). The torsion

angles of the GalNAc–Gal glycosidic linkage of this tetrasaccharide populated one cluster with averaged angles (Φ, Ψ) = (30° ± 12°, 17° ± 13°). In contrast, two clusters of the torsion angles of the Neu5Ac–Gal linkage, (Φ, Ψ) = (−174° ± 11°, −32° ± 11°) and (−69° ± 10°, −6° ± 14°), and three clusters of the Gal–Glc linkage, (Φ, Ψ) = (−34° ± 15°, −32° ± 17°), (40° ± 11°, −4° ± 20°) and (37° ± 21°, −167° ± 19°), were observed.

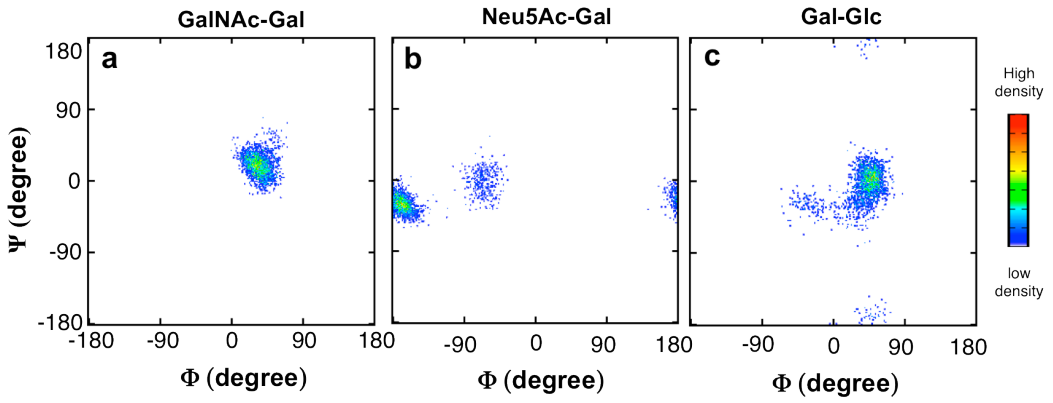


**Figure 3.1.** Torsion angle density maps of the 2,000 trisaccharide conformers of (**a**, **b**, and **c**) GM2 tetrasaccahride (**a**) The GalNAc–Gal, (**b**) the Neu5Ac–Gal, and (**c**) the Gal–Glc linkages. The definitions of Φ and Ψ were used for the GalNAc–Gal and the Gal–Glc linkages, Φ = H1–C1–O'4–C'4 and Ψ = C1–O'4–C'4–H'4, and the Neu5Ac–Gal linkage, Φ = C1–C2–O'3–C'3 and Ψ = C2–O'3–C'3–H'3.

**3D Structural information observation:**

To evaluate the conformation dynamics of the GM2 tetrasaccharide, PCS analyses of the oligosaccharide were performed. The paramagnetic lanthanide tag was introduced to the GM2 tetrasaccharide, as shown in Scheme 3.1. The reducing terminus of the tetrasaccharide was aminated in good yield by selective azidation and subsequent reduction reactions, and then covalently attached to a phenylenediamine derivative. The PCS (Δδ) values of $^{1}H$ and $^{13}C$ were measured as the differences between the chemical shifts of the compound chelated to the paramagnetic ion such as $Tm^{3+}$ and those observed with the diamagnetic ion $La^{3+}$ in their $^{1}H$–$^{13}C$ HSQC spectra (Figure 3.2, Table 3.1 and Table 3.2).

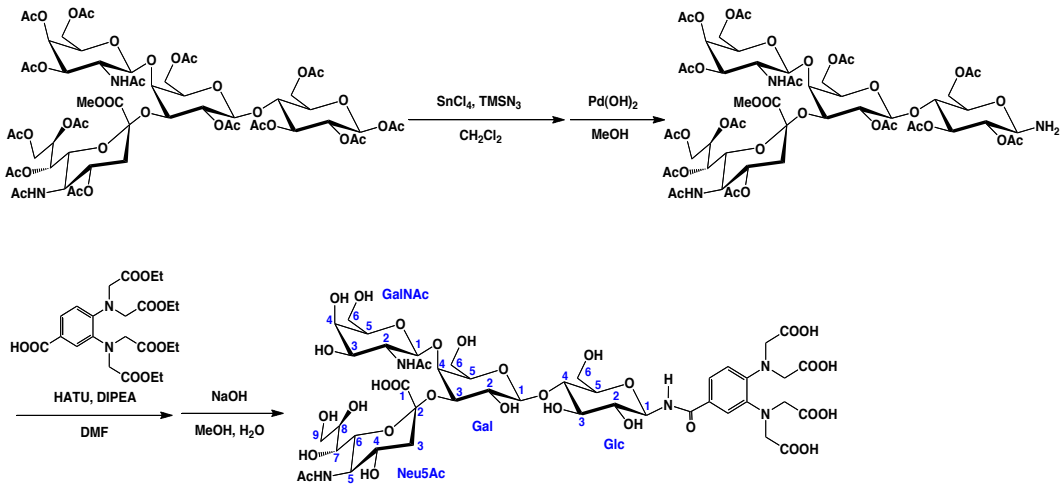


**Scheme 3. 1.** Paramagnetic tagging of the GM2 tetrasaccharide

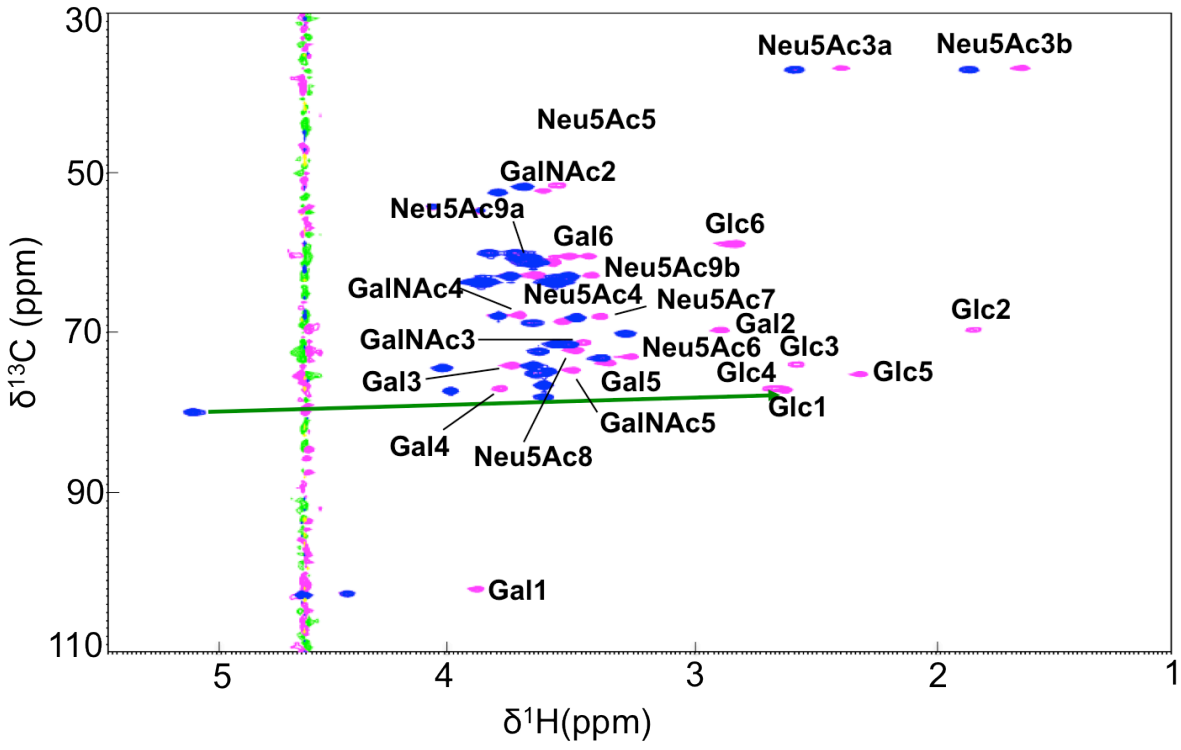


**Figure 3.2.** $^{1}H–^{13}C$ HSQC spectra of the GM2 tetrasaccharide tagged with $Tm^{3+}$ (magenta) and $La^{3+}$ (blue).

**Table 3.1**. $^{1}H$ and $^{13}C$ chemical shifts of the GM2 tetrasaccharide tagged with $La^{3+}$, $Tm^{3+}$, and $Tb^{3+}$ ions. [(a)] Not detected due to low S/N ratio.

| | $La^{3+}$ | | $Tm^{3+}$ | | $Tb^{3+}$ | |
|---|---|---|---|---|---|---|
| | **$\delta^{13}C$ /ppm** | **$\delta^{1}H$ /ppm** | **$\delta^{13}C$ /ppm** | **$\delta^{1}H$ /ppm** | **$\delta^{13}C$ /ppm** | **$\delta^{1}H$ /ppm** |
| **Glc 1** | 79.95 | 5.132 | 77.12 | 2.620 | n.d.[(a)] | n.d. |
| **2** | 71.44 | 3.547 | 69.57 | 1.811 | n.d. | n.d. |
| **3** | 75.15 | 3.676 | 73.93 | 2.565 | n.d. | n.d. |
| **4** | 78.06 | 3.652 | 76.94 | 2.670 | 75.97 | 1.683 |
| **5** | 76.63 | 3.652 | 75.17 | 2.295 | n.d. | n.d. |
| **6** | 59.99 | 3.884 | 58.86 | 2.840 | 58.01 | 2.049 |
| **6** | 59.98 | 3.772 | 58.86 | 2.800 | 58.01 | 1.939 |
| **Gal 1** | 102.7 | 4.480 | 102.1 | 3.922 | 101.6 | 3.325 |
| **2** | 70.10 | 3.305 | 69.65 | 2.890 | 69.20 | 2.416 |
| **3** | 74.43 | 4.074 | 74.09 | 3.778 | 73.75 | 3.419 |
| **4** | 77.31 | 4.046 | 77.00 | 3.823 | 76.63 | 3.514 |
| **5** | 74.12 | 3.698 | 73.75 | 3.360 | 73.34 | 2.932 |
| **6** | 60.67 | 3.751 | 60.39 | 3.530 | 60.00 | 3.142 |
| **6** | 60.66 | 3.702 | 60.39 | 3.480 | 60.00 | 2.985 |
| **Neu5Ac 3** | 36.98 | 2.590 | 36.77 | 2.393 | 36.64 | 2.143 |
| **3** | 36.99 | 1.844 | 36.76 | 1.612 | 36.64 | 1.346 |
| **4** | 68.78 | 3.700 | 68.57 | 3.570 | 68.44 | 3.409 |
| **5** | 51.66 | 3.731 | 51.47 | 3.577 | 51.39 | 3.403 |
| **6** | 73.15 | 3.405 | 72.96 | 3.275 | 72.81 | 3.103 |
| **7** | 68.11 | 3.508 | 67.92 | 3.407 | 67.81 | 3.263 |
| **8** | 72.37 | 3.669 | 72.18 | 3.505 | 72.03 | 3.285 |
| **9** | 62.90 | 3.792 | 62.76 | 3.677 | 62.64 | 3.516 |
| **9** | 62.90 | 3.543 | 62.75 | 3.441 | 62.64 | 3.289 |
| **GalNAc 1** | 102.8 | 4.680 | 102.6 | 4.480 | 102.3 | 4.227 |
| **2** | 52.40 | 3.845 | 52.17 | 3.641 | 51.97 | 3.324 |
| **3** | 71.38 | 3.594 | 71.20 | 3.470 | 71.02 | 3.278 |
| **4** | 67.88 | 3.844 | 67.71 | 3.747 | 67.54 | 3.564 |
| **5** | 74.82 | 3.637 | 74.64 | 3.524 | 74.45 | 3.315 |
| **6** | 61.23 | 3.693 | 61.10 | 3.609 | 60.93 | 3.405 |

**Table 3.2.** PCS values (ppm) derived from the $Tm^{3+}$ ion.

| | Glc | | Gal | | Neu5Ac | | GalNAc | |
|---|---|---|---|---|---|---|---|---|
| | $\Delta\delta^{13}C$ | $\Delta\delta^{1}H$ | $\Delta\delta^{13}C$ | $\Delta\delta^{1}H$ | $\Delta\delta^{13}C$ | $\Delta\delta^{1}H$ | $\Delta\delta^{13}C$ | $\Delta\delta^{1}H$ |
| **1** | −2.83 | −2.51 | −0.62 | −0.56 | | | −0.23 | −0.20 |
| **2** | −1.87 | −1.74 | −0.45 | −0.41 | | | −0.23 | −0.20 |
| **3** | −1.22 | −1.11 | −0.34 | −0.30 | −0.22 | −0.23/−0.20 | −0.18 | −0.12 |
| **4** | −1.12 | −0.98 | −0.31 | −0.22 | −0.22 | −0.13 | −0.16 | −0.10 |
| **5** | −1.46 | −1.36 | −0.36 | −0.34 | −0.20 | −0.15 | −0.17 | −0.11 |
| **6** | −1.12 | −1.04/−0.97 | −0.27 | −0.22 | −0.19 | −0.13 | −0.13 | −0.08 |
| **7** | | | | | −0.18 | −0.10 | | |
| **8** | | | | | −0.19 | −0.16 | | |
| **9** | | | | | −0.15 | −0.11/−0.10 | | |

**Comparison of experimental and back–calculated PCS:**

The ensemble model of the tetrasaccharide was created by extracting the 2,000 conformers at equal intervals from the combined MD trajectory, involving transitions from a low–energy region to another in the energy landscape. According to the previously reported method [5], the PCS values of the tetrasaccharide with $Tm^{3+}$ were back–calculated using this ensemble model. The expected PCS values were in excellent agreement with the experimental value, with a low $Q$ value = 0.06 (Figure 3.3), which clearly validated the atomic description of this branched tetrasaccharide. $Q = \text{rms}(\Delta\delta_{calc} - \Delta\delta_{obs})/\text{rms}(\Delta\delta_{obs})$. $\Delta\delta_{calc}$ is given by following equation:

$$\Delta\delta_{calc} = \Sigma_{i=1}^{N}(p_i \cdot \frac{1}{12}\pi r_i^3 \cdot [\Delta\chi_{ax}(3\cos^2\theta_i - 1) + \frac{3}{2} \cdot \Delta\chi_{rh}(\sin^2\theta_i \cos 2\varphi_i)])$$

where $p_i$ is populations of each structure (set to 0.0005), $N$ is number of each conformers, and ($r_i$, $\theta_i$, $\varphi_i$) defines the position vector for conformer $i$ of the nucleus in polar coordinates with respect to the metal center and principal axis of $\Delta\chi$ tensor.

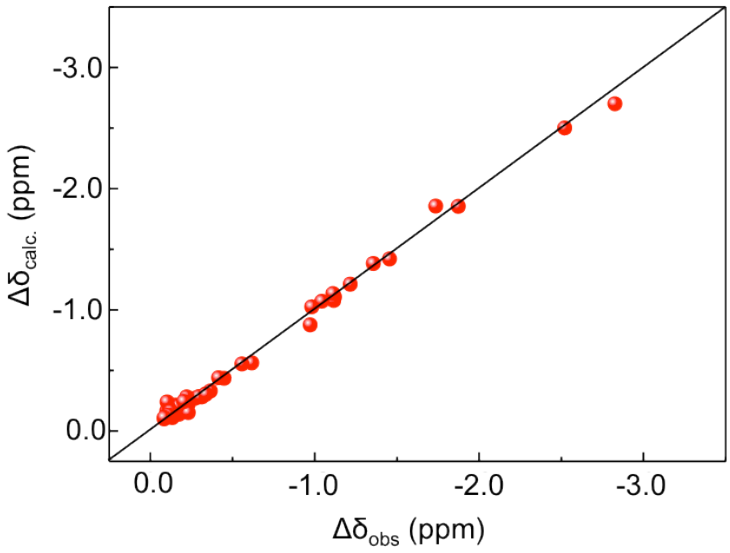


**Figure 3.3.** Correlations between the experimentally observed and back–calculated PCS values of the GM2 tetrasaccharide with $Tm^{3+}$.

The most populated conformation of the GM2 tetrasaccharide was similar to the previously reported structure, determined by the inspection of the NOEs observed in DMSO [7a] and those predicted by theoretical calculations [7]. Especially, the GalNAc–Gal moiety showed a rigid conformation with a single cluster, which is consistent with these reports. It is plausible that the bulky acetyl group of the GalNAc residue restricts the motional freedom of this glycosidic linkage. The Neu5Ac–Gal glycosidic linkage has two conformational clusters, which were similarly indicated in previous studies using Monte Carlo–based calculations [7d] and an MD simulation with another force field [7e].

### 3.2.2 Analyses of the conformational dynamics of GM1 pentasaccharide

**MD simulation of GM1 pentasaccharide:**

All–atom MD simulations with the GLYCAM_06 force field [6] were employed to capture the conformational dynamics of the sugar moiety of GM1. Ten MD simulations were performed in explicit water for 12 ns at 300 K to generate the atomic coordinates of the GM1 pentasaccharide. All MD runs were combined after excluding the first 2 ns of trajectories.

Subsequently, 2,000 pentasaccharide conformers were extracted at equal intervals to create an ensemble model, and the glycosidic torsion angles were monitored (Figure 3.4a, 3.4b, 3.4c and 3.4d). In the torsion angle density maps from MD simulation of GM2 and GM1, population differences of major conformers, especially in the Neu5Ac–Gal glycosidic linkage were shown (Figure 3.1b and Figure 3.4c).

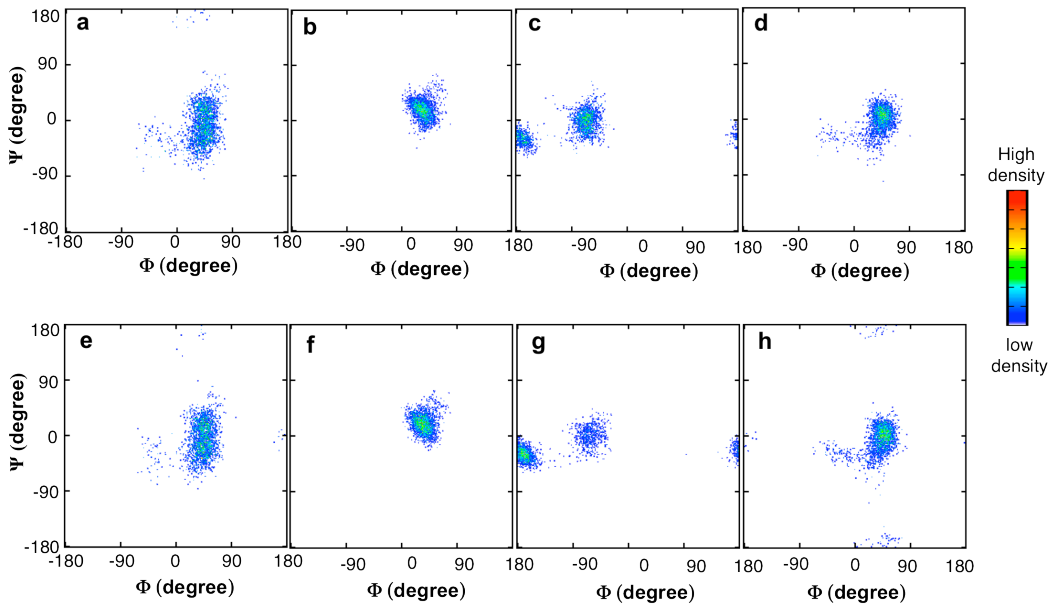


**Figure 3.4**. Torsion angle density maps of GM1 pentasaccharide, MD simulation results (**a, b, c, d**) and REMD results (**e, f, g, h**). Gal–GalNAc (**a** and **e**), GalNAc–Gal (**b** and **f**), Neu5Ac–Gal (**c** and **g**), and Gal–Glc ((**d** and **f**) linkages. The definitions of Φ and Ψ were used for the Gal–GalNAc, GalNAc–Gal and the Gal–Glc linkages, Φ = H1–C1–O'4–C'4 and Ψ = C1–O'4–C'4–H'4, and the Neu5Ac–Gal linkage, Φ = C1–C2–O'3–C'3 and Ψ = C2–O'3–C'3–H'3.

To validate the simulation results of GM1 pentasaccharide, experimental data was collected. PCSs of GM1 pentasaccharide were measured by using tagged GM1, as showing in scheme 3.2. GM1 pentasaccharide firstly was release from commercial available GM1 gangliosides by using enzymatic reaction. Then the reducing terminus OH group was changed to $NH_2$ group in the presence of excess $NH_4HCO_3$. Finally, the lanthanide tag was

attached to GM1 oligosaccharide through rigid amido linkage to intoroduce the paramagnetic probe. The PCS (Δδ) values of $^{1}H$ and $^{13}C$ were measured as the differences between the chemical shifts of the compound chelated to the paramagnetic $Tm^{3+}$ ion and those observed with the diamagnetic $La^{3+}$ ion in their $^{1}H$–$^{13}C$ HSQC spectra (Table 3.3 and Figure 3.5).

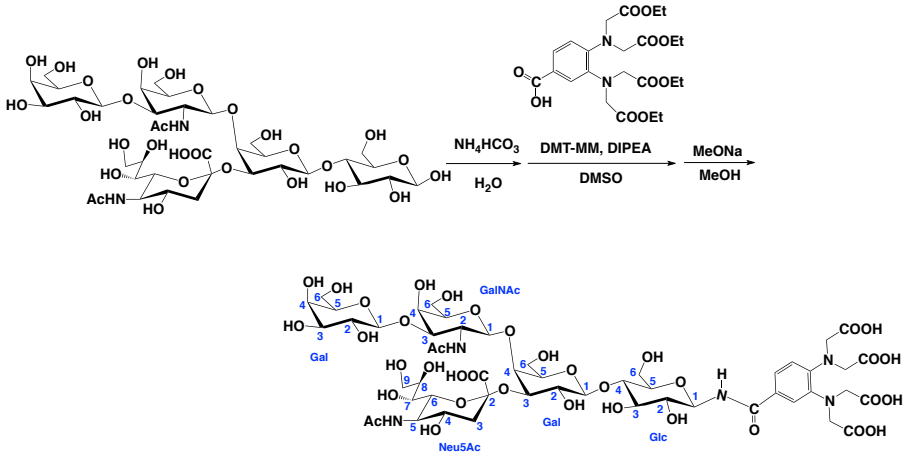


**Scheme 3.2.** Paramagnetic tagging of the GM1 pentasaccharide

**Table 3.3.** PCS values (ppm) of GM1 pentasaccharide derived from the $Tm^{3+}$ ion.

| | **Glc** | | **GalI** | | **Neu5Ac** | | **GalNAc** | | **GalII** | |
|---|---|---|---|---|---|---|---|---|---|---|
| | **$\Delta\delta^{13}C$** | **$\Delta\delta^{1}H$** | **$\Delta\delta^{13}C$** | **$\Delta\delta^{1}H$** | **$\Delta\delta^{13}C$** | **$\Delta\delta^{1}H$** | **$\Delta\delta^{13}C$** | **$\Delta\delta^{1}H$** | **$\Delta\delta^{13}C$** | **$\Delta\delta^{1}H$** |
| **1** | –2.71 | –2.52 | –0.63 | –0.56 | | | –0.15 | –0.18 | –0.07 | –0.11 |
| **2** | –1.86 | –1.75 | –0.42 | –0.42 | | | –0.19 | –0.21 | –0.07 | –0.08 |
| **3** | –1.19 | –1.10 | –0.32 | –0.3 | –0.19 | –0.21 | –0.09 | –0.12 | –0.06 | –0.08 |
| **4** | –1.01 | –0.99 | –0.20 | –0.22 | –0.11 | –0.13 | –0.11 | –0.09 | –0.03 | –0.06 |
| **5** | –1.41 | –1.34 | –0.31 | –0.31 | –0.09 | –0.14 | –0.08 | –0.11 | –0.07 | –0.07 |
| **6** | –1.10 | –1.04/–0.94 | –0.27 | –0.24 | –0.09 | –0.13 | –0.71 | –0.14 | | |
| **7** | | | | | –0.11 | –0.10 | | | | |
| **8** | | | | | –0.11 | –0.15 | | | | |
| **9** | | | | | –0.12 | –0.10 | | | | |

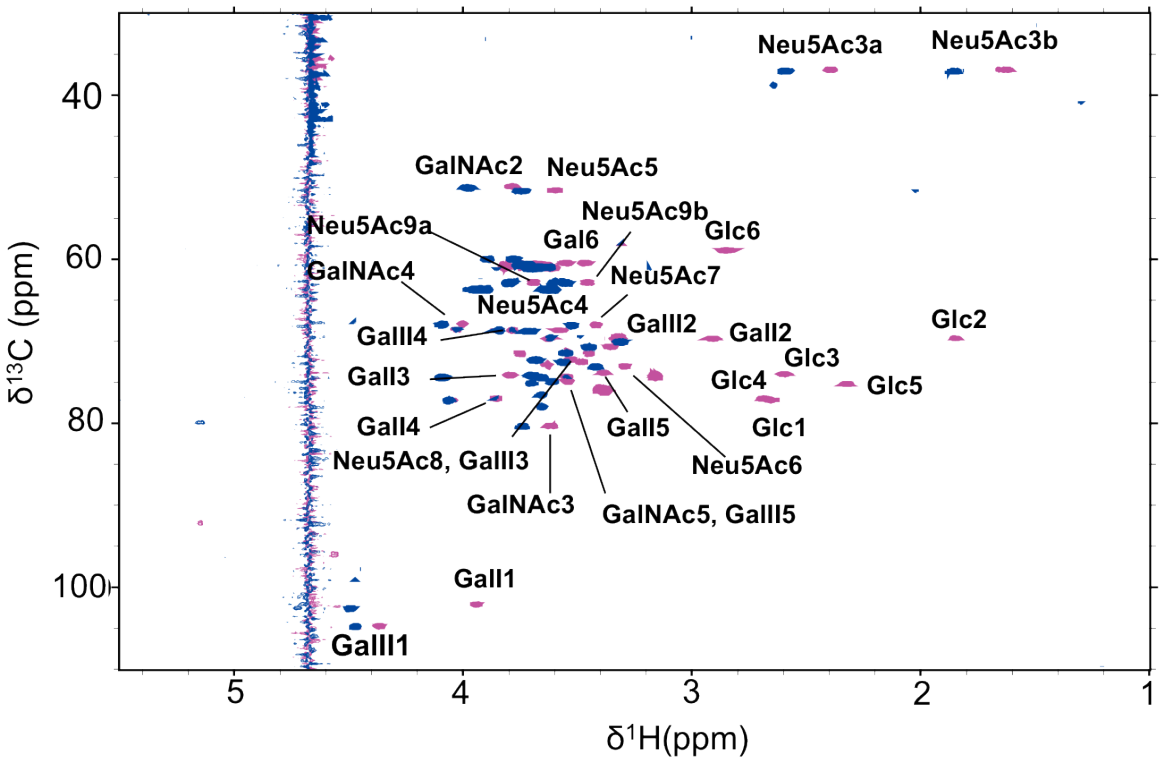


**Figure 3.5.** $^{1}H–^{13}C$ HSQC spectra of the GM1 pentasaccharide tagged with $Tm^{3+}$ (magenta) and $La^{3+}$ (blue).

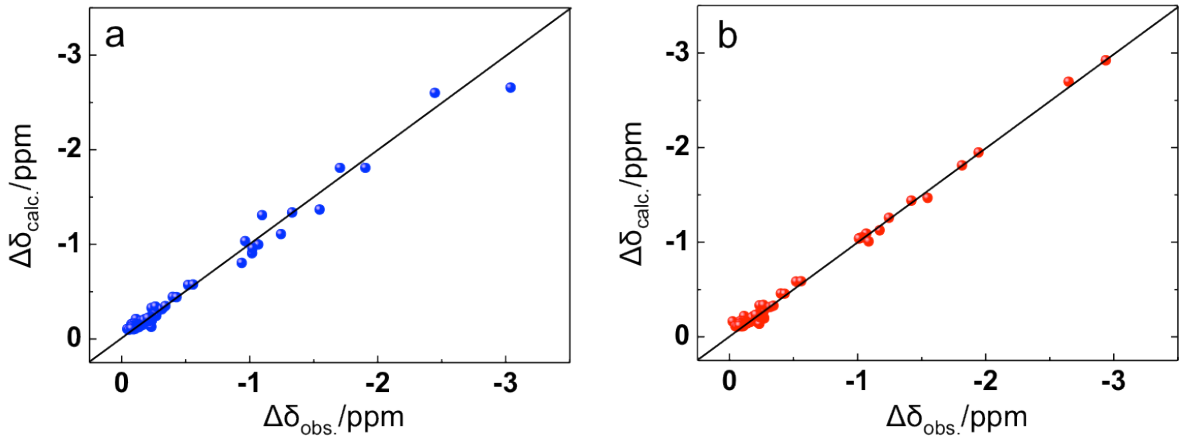


**Figure 3.6.** Correlations between the experimentally observed and back–calculated PCS values based on the conventional MD simulation ensemble (a) and REMD simulation ensemble (b) of the GM1 pentasaccharide with $Tm^{3+}$

The experimental data was compared with the back calculated PCS based on the conformational ensemble generated by MD simulation, with $Q$ = 0.137 (Figure 3.6a). This $Q$ value is much larger than GM2 and GM3 cases. The fitting did not become better even by increasing the simulation time to 240 ns. The reason for the mismatch probably is the insufficient sampling caused by energy barriers between the multiple minima in overall conformational space of large branched oligosaccharides. These multiple conformers cannot be accessed completely by conventional MD simulation even within nanosecond time–scale. Recently, replica exchange MD (REMD) simulation was considered to be powerful to overcome the sampling problems of large oligosaccharides [8] by employing a set of replicated simulations at different temperature to avoid being trapped into a local energy minimum. Hence, to explore a larger space and enhance the conformational sampling, REMD simulation of GM1 pentasaccharide was performed.

**REMD simulation of GM1 pentasaccharide:**

REMD simulations for GM1 pentasaccharide were carried out with the GLYCAM_06 force field and TIP3P water model. 32 replicas were used with temperature ranging from 300 K to 500 K. MD simulation of 60 ns was performed for each replica. The torsion angles of GM1 pentasaccharide analyzed from 2,000 conformers based on the REMD simulation results were shown in Figure 3.4 (Figure 3.4f, 3.4h, 3.4g and 3.4i). Conformational differences of glycosidic linkage of Neu5Ac–Gal (Figure 3.4c and Figure 3.4g) and Gal–Glc (Figure 3.4d and Figure 3.4h) were found in the simulation results of GM1 pentasaacharide given by MD and REMD. For Neu5Ac–Gal linkage, both simulations provided two major clusters of torsion angles, but the distributions were obviously different. Moreover, the minor conformers of Gal–Glc linkage with ($\Phi$, $\Psi$) = (37° ± 21°, −167° ± 19°) was shown up in REMD simulation but not in conventional MD simulation.

The experimental PCS data was used to validate this REMD simulation result. The back–calculated PCS of the GM1 pentasaccharide with $Tm^{3+}$ from REMD results was in good agreement with the experimental PCS data with a lower $Q$ = 0.072 [Figure 3.6b]. As mentioned above, although the simulation results of GM1 pentasaccahride were affected by calculation conditions, PCS played as potent tool for validating the simulation results and thus provide us the accurate conformational dynamics of oligosaccharides.

### 3.2.3 Conformational difference among GM1, GM2 and GM3 glycans

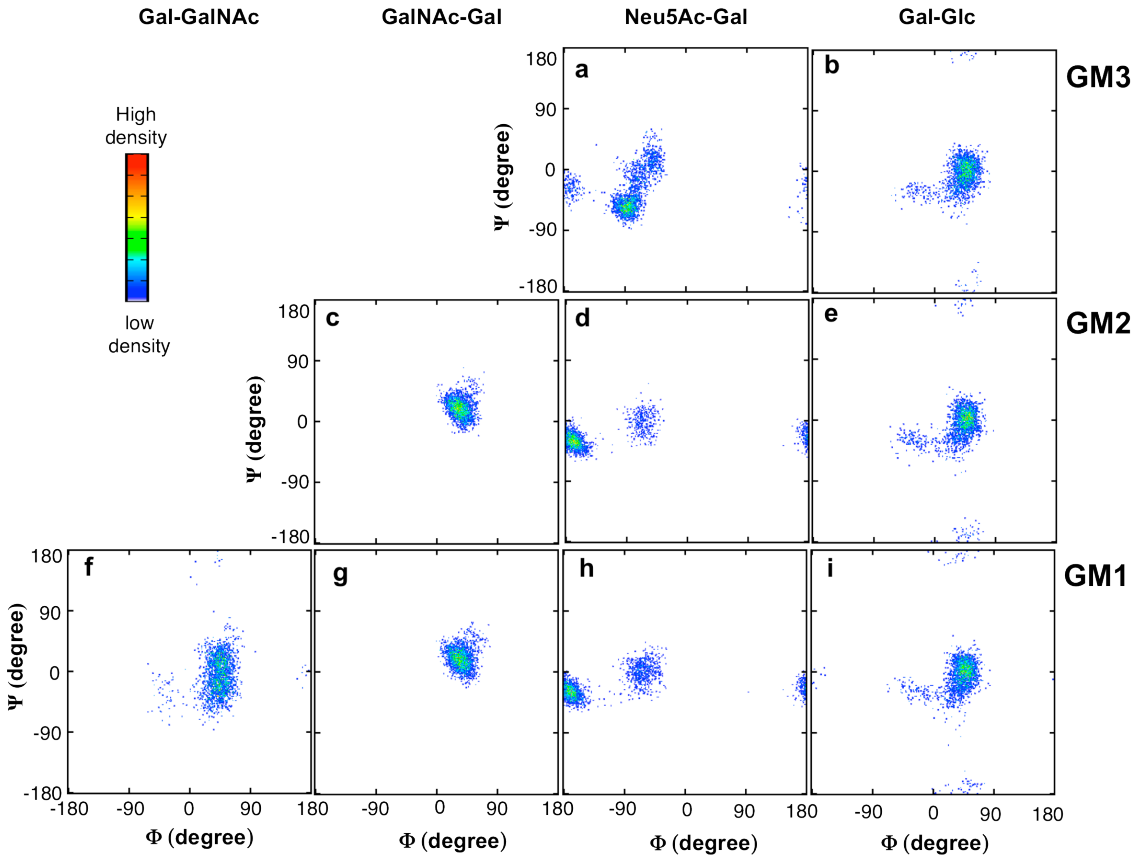


**Figure 3.7**. Torsion angle density maps of GM3 trisaccharide (**a and b**) and GM2 tetrasaccharide (**c, d and e**) generated by MD simulation and GM1 pentasaccharide (**f, g, h and i**) generated by REMD simulation. The Gal–GalNAc (**f**), the GalNAc–Gal (**c** and **g**), the Neu5Ac–Gal, and (**a, d and h**) and the Gal–Glc (**b, e and i)** linkages. The definitions of Φ and Ψ were used for the Gal–GalNAc, GalNAc–Gal and the Gal–Glc linkages, Φ = H1–C1–O'4–C'4 and Ψ = C1–O'4–C'4–H'4, and the Neu5Ac–Gal linkage, Φ = C1–C2–O'3–C'3 and Ψ = C2–O'3–C'3–H'3.

The conformational spaces of GM1 pentasaccharide, GM2 tetrasaccharide and GM3 trisaccharide were compared. The inner part of GM1 pentasaccharide and GM2 tetrasaccharide share the similar conformational space, as the simulation result shown in Figure 3.7. This result is consistence with the experimental PCSs of GM1 pentasaccharide and GM2 tetrasaccharide with $Tm^{3+}$ (Figure 3.8, green bar) where no significant PCS difference was observed between GM2 tetrasaccharide and GM1 pentasaccharide.

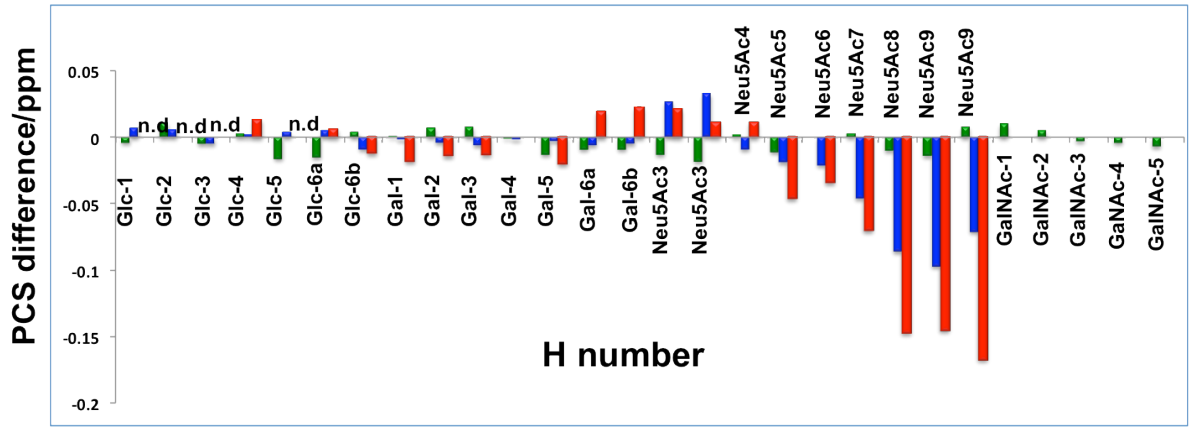


**Figure 3.8.** The differences of proton PCS values shown as subtraction of $\Delta\delta^1H$ of the GM2 tetrasaccharide from $\Delta\delta^1H$ of the GM1 pentasaccharide with $Tm^{3+}$ (green), from $\Delta\delta^1H$ of the GM3 trisaccharide with $Tm^{3+}$ (blue) and $Tb^{3+}$ (red). n.d., not detected due to extensive line broadening.

However, both simulation (Figure 3.7) and PCS data (Figure 3.8) show the conformational differences between branched GM2 trisaccharide and linear GM3 trisaccharide. To examine the impact of the additional GalNAc branch on the conformational space of the other part of the GM2 glycan, the experimental proton PCS data and the simulated glycosidic torsion angles were compared between the GM2 and GM3 oligosaccharides. The Neu5Ac residues exhibited significant differences in the PCS induced by $Tm^{3+}$ or $Tb^{3+}$; however, there were marginal differences between the Gal and Glc residues

(Figure 3.8). These data suggest that the conformation of the sialyl linkages is different between the GM2 tetrasaccharide and the GM3 trisaccharide, whereas the conformation of the inner lactose part of the ganglioside is slightly affected by attaching the outer GalNAc residue. In agreement with the PCS data, the simulated ensemble of the Gal–Glc linkage torsion angles was very similar between the GM2 tetrasaccharide and GM3 trisaccharide (Figure 3.7b and 3.7e). In contrast, significant differences were observed in the simulated conformational ensemble of the Neu5Ac–Gal glycosidic linkages. In the GM3 trisaccharide, the conformations of this linkage is most populated in the cluster (Φ, Ψ) = (−90° ± 11°, −57° ± 11°), while the corresponding cluster is missing in the GM2 tetrasaccharide (Figure 3.7a and 3.7d). This suggests that the additional GalNAc branch restricts the conformational freedom of the Neu5Ac–Gal glycosidic linkage in the GM2 tetrasaccharide. The conformation of the Neu5Ac–Gal moiety with the torsion angles (Φ, Ψ) = (−90° ± 11°, −57° ± 11°) was sterically hindered by the GalNAc residue in the branched GM2 tetrasaccharide. To avoid the steric hinderance, the torsion angles of the Neu5Ac–Gal linkage are populated in the other clusters, (Φ, Ψ) = (−174° ± 11°, −32° ± 11°) and (−69° ± 10°, −6° ± 14°) in the GM2 tetrasaccharide. In the former conformational cluster, the side chain of Neu5Ac consisted of the C7, C8, and C9 groups oriented in spatial proximity to the GalNAc residue, presumably with preferable interactions between these residues, as indicated in previous reports [7a, 7c]. For example, structural arrangements in which the hydroxyl group at C8 or C9 of the Neu5Ac residue and the hydroxyl group at C6 of the GalNAc residue are close to each other are frequently observed in the MD trajectory. In addition, atomic contacts were observed between the GalNAc amide group and the Neu5Ac carboxylate group, suggesting the transient formation of a hydrogen bond between these groups, which was observed in the DMSO solution [9] (Figure 3.9). Hence, the stabilization of the major conformations of the GM2 sialyl linkage can be attributed to these inter–residue interactions [10]. In the

metastable conformational cluster of the GM2 sialyl linkage, a water molecule was frequently found between the Neu5Ac side chain and the GalNAc residue, maintaining the distance between the Neu5Ac carboxylate and GalNAc amide groups. The observed differences in the conformational space of the Neu5Ac–Gal linkage between the GM2 and GM3 sugar chains are qualitatively consistent with the results of the MD calculations of the sugar moieties of GM2 and GM3 employing another force field [7e] and the Monte Carlo–based calculations of the GM2 headgroup and the αNeu5Ac–(2–3)–Gal disaccharide [7d].

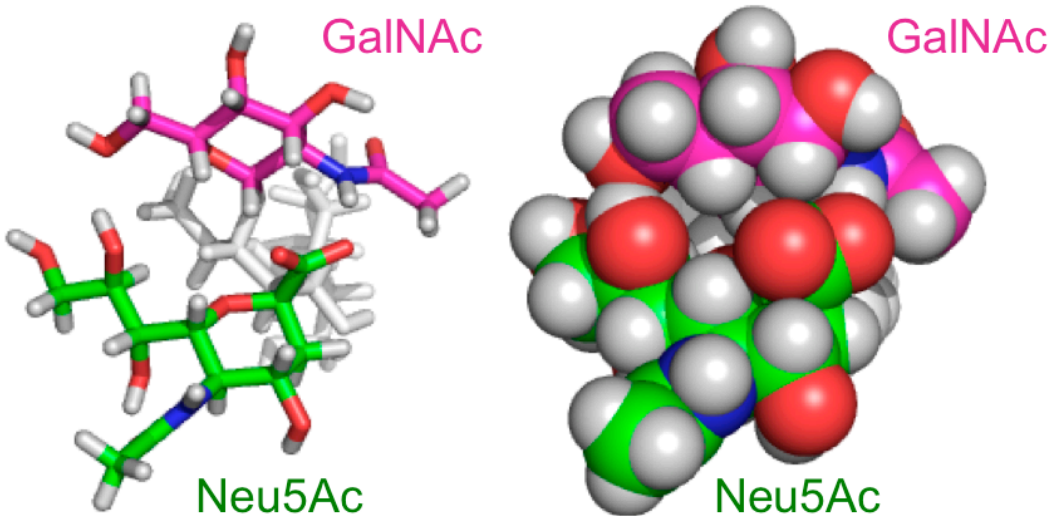


**Figure 3.9.** Three–dimensional structural model of one of the major conformers of the GM2 tetrasaccharide. Cylinder (**left**) and space–filling (**right**) models are shown in the same orientation.

## 3.3 Conclusions

In summary, the lanthanide–assisted NMR approach was successfully applied to the characterization of the conformational dynamics of the branched glycans of GM2 and GM1. PCS data was employed as a powerful tool to validate the simulation results, which will be beneficial for making the improvement on computational simulation. In addition, the inter–branch interactions that are responsible for the conformational differences between the

branched oligosaccharides (GM2 tetrasaccahride and GM1 pentasaccharide) and the linear oligosaccharide (GM3 trisaccharide) were identified by this paramagnetic NMR method in conjunction with computational simulations. The success of this systematic approach opens new prospects for the conformational analysis of dynamic structures of more complex, high–antennary oligosaccharides toward decoding glycocodes from 3D structural aspects. In addition, the lanthanide tagging approach serve as an experimental tool for validating MD simulations of not only oligosaccharides but also other flexible biomacromolecules such as intrinsically disordered proteins.

## 3.4 Material and Experiments

### 3.4.1 General

Reagents and solvents were commercially available and used without any further purification unless otherwise noted. Column chromatography was performed using Silica Gel 60N purchased from Kanto Chemical Co., Inc., Wakosil 40C18 from Wako Pure Chemical Industries, Ltd., or Waters Sep–Pak C18. High–resolution MS measurements were performed on a JEOL JMS–777V spectrometer (Akishima, Japan). The NMR spectra were recorded on a JEOL JNM ECA–600 spectrometer equipped with a 5–mm FG/HCN probe. TMS (in CDCl3) served as internal standard for the $^{1}$H– and $^{13}$C–NMR measurements.

### 3.4.2 Simulations

#### 3.4.2.1 MD Simulations of GM2 tetrasaccharide and GM1 pentasaccharide

All–atom MD simulations of the GM2 tetrasaccharide and GM1 pentasaccharide were employed using the Sander module of the Amber11 package [11] with the GLYCAM_06 force field. To create the topology file of the GM2 tetrasaccharide, the tLeap module of the AmberTools1.5 program was used. The initial structure for GM2 was determined on the basis

of preliminary MD calculations, in which the glycosidic torsion angles Φ and Ψ were 39.8° and −43.6° for Gal–Glc, 42.1° and 16.9° for GalNAc–Gal, and −175.2° and −25.6° for Neu5Ac–Gal linkages. For GM1 pentasaccharide, the initial structure were generate by the tLeap module of the AmberTools1.5 program, with glycosidic torsion angles Φ and Ψ 60.05° and −60.36° for Gal–Glc, 60° and 60.14° for GalNAc–Gal, 60° and 60.35° for Gal–GalNAc and −128.42° and −61.35° for Neu5Ac–Gal linkages. TIP3P waters were added to the solvent layer to ensure a depth of at least 8 Å from any atom and ten $Na^+$ ions and nine $Cl^-$ ions were added to neutralize the system. The simulation system of GM2 tetrasaccharide contained 737 water molecules bringing total 2,338 atoms. The simulation system of GM1 pentasaccharide contained 801 water molecules bringing total 2,551 atoms. Before the MD runs were performed, the entire system energy was minimized by 500 steps of the steepest decent followed by 500 steps of the conjugate gradient. The system was heated to 300 K with a 2–fs time step in the NPT ensemble [12] at 1 atm over 50 ps using isotropic position scaling. Productive MD simulations were performed for 12 ns at 300 K with a 2–fs time step in the NPT ensemble. The initial velocities were randomized. The scaling of nonbonded 1–4 van der Waals and electrostatic interactions was not performed (*i.e.*, SCEE = SCNB = 1.0). All bonds involving hydrogen atoms were constrained using the SHAKE algorithm [13], and long–range electrostatics were treated by the particle–mesh Ewald method [14]. Snapshots were collected every 1 ps. Ten MD trajectories excluding the first 2 ns were combined into one. The analysis of the trajectories was performed using the PTRAJ module of the AmberTools1.5 program, and molecular graphics images were produced using VMD [15].

#### 3.4.2.2 REMD Simulations of GM1 pentasaccharide

REMD simulations were carried out by using Amber12 package with the GLYCAM_06 force field and TIP3P water model. The simulation system contained total

2551 atoms, including 801 water molecules, ten $Na^+$ ions and nine $Cl^-$ ions. Thirty–two replicas were used with temperature ranging from 300 K to 500 K. All bonds involving hydrogen atoms were constrained using the SHAKE algorithm [13], and long–range electrostatics were treated by the particle–mesh Ewald method [14]. MD simulation of 60 ns was performed with a 2–fs time step for each replica. The total simulation time is 1.9 μs (60–ns x 32 = 1920–ns) for the system.

### 3.4.3 Preparation of the tagged oligosaccharides

#### 3.4.3.1 Preparation of the tagged GM2 tetrasaccharide

**Preparation of azide 2:**

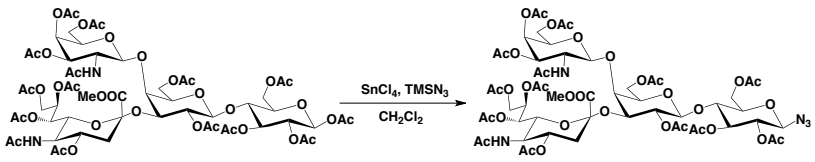


**1** **2**

Trimethylsilyl azide (468 μL, 3.56 mmol) and $SnCl_4$ (218.5 μL, 1.86 mmol) was added to a solution of compound **1** (600 mg, 0.437 mmol) in $CH_2Cl_2$ (5 mL) at 0 °C. The mixture was stirred at RT for 12 h. Then, the reaction mixture was diluted with $CHCl_3$, washed with saturated aqueous $NaHCO_3$, $H_2O$, dried with $Na_2SO_4$, and concentrated. The residue was purified by column chromatography on silica gel ($CHCl_3$/MeOH 20:1) to give **2** (528 mg, 89%). $^1$H–NMR (600 MHz, $CDCl_3$, 300 K): δ = 5.98 (d, *J* = 6.90 Hz, GalNAc–NH), 5.83 (dd, *J* = 3.4, 11.0 Hz, 1H, GalNAc–H3), 5.53 (m, 1H, Neu5Ac–H8), 5.35 (m, 2H, Neu5Ac–H7, GalNAc–H4), 5.17 (t, *J* = 9.67 Hz, 1H, Glc–H3), 5.13 (d, *J* = 8.23 Hz, 1H, GalNAc–H1), 5.05 (d, *J* = 10.3Hz, 1H, Neu5Ac–NH), 4.97 (dd, *J* = 7.57, 10.3 Hz, 1H, Gal–H2), 4.86 (t, *J* = 9.26 Hz, 1H, Glc–H2), 4.81 (m, 1H, Neu5Ac–H4), 4.61 (m, 2H, Gal–1H, Glc–1H), 4.49 (m, 1H, Glc–H6a), 4.34 (dd, *J* = 2.75, 13.0 Hz, 1H, Neu5Ac–H9a), 4.22 (m, 2H, GalNAc–H6a,

Gal–H3), 4.12–3.93 (m, 6H, GalNAc–H6b, Neu5Ac–H9b, Glc–H6b, Gal–H6, Neu5Ac–H5), 3.83 (m, 6H, Glc–H4, Gal–H5, Neu5Ac–H6, Neu5Ac–$COOCH_3$), 3.68 (m, 1H, Glc–H5), 3.59 (t, *J* = 5.82 Hz, 1H, GalNAc–H5), 3.50 (d, *J* = 2.06 Hz, 1H, Gal–H4), 3.38 (m, 1H, GalNAc–H2), 2.81 (dd, *J* = 4.34, 13.3 Hz, 1H, Neu5Ac–H3a), 2.21–1.77 (m, 42H, OAc, NHAc ), 1.72 (t, *J* = 12.5 Hz, Neu5Ac–H3b). $^{13}$C–NMR (150 MHz, $CDCl_3$, 300 K): δ = 171.3, 171.0, 170.3, 169.9, 168.8, 100.6, 99.25, 87.78, 75.48, 74.97, 73.54, 73.02, 72.94, 72.20, 71.92, 71.08, 70.24, 69.59, 68.62, 67.55, 66.83, 63.38, 62.27, 62.06, 61.50, 53.05, 52.93, 49.43, 37.36, 25.52, 23.20, 21.60, 20.97, 20.69. HRMS (FAB): Calcd for $C_{56}H_{78}N_5O_{35}$ [M+H$^+$]: 1380.4399; Found: 1380.4484.

**Preparation of amine 3:**

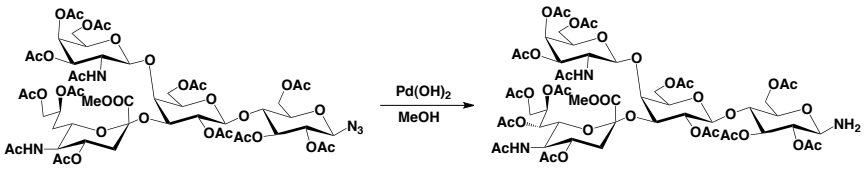


**2** **3**

Compound **2** (528 mg, 0.383 mmol) was dissolved in MeOH (5 mL), and to this solution, Pd/C (10 mg) was added. The mixture was stirred in a hydrogen atmosphere at RT for 12 h. The reaction mixture was filtered through celite, concentrated, and then purified by column chromatography on silica gel ($CHCl_3$/MeOH 20:1) to give **3** (460 mg, 78%). $^1$H–NMR (600 MHz, $CDCl_3$, 300 K): δ = 6.14 (d, *J* = 6.87 Hz, 1H, GalNAc–NH), 5.88 (dd, *J* = 3.50, 11.3 Hz, 1H, GalNAc–H3), 5.51 (m, 1H, Neu5Ac–H8), 5.36 (m, 2H, Neu5Ac–H7, GalNAc–H4), 5.16 (m, 2H, Glc–H3, GalNAc–H1), 5.05 (d, *J* = 10.3 Hz, 1H, Neu5Ac–NH), 4.97 (dd, *J* = 7.72, 10.3 Hz, 1H, Gal–H2), 4.79 (m, 1H, Neu5Ac–H4), 4.73 (t, *J* = 9.30 Hz, 1H, Glc–H2), 4.57 (d, *J* = 7.96 Hz, 1H, Gal–H1), 4.44 (d, *J* = 11.4 Hz, 1H, Glc–H6a), 4.34 (dd, *J* = 2.84, 13.2 Hz, 1H, Neu5Ac–H9a), 4.21 (m, 2H, GalNAc–H6a, Gal–H3), 4.15–3.93 (m, 7H, Gal6, GalNAc–H6b, Neu5Ac–H9b, Glc–H6b, Neu5Ac–H5, Glc–H1), 3.86–3.74 (m, 6H, Neu5Ac–

$COOCH_3$, Gal–H5, Neu5Ac–H6, Glc–H4), 3.58 (m, 2H, GalNAc–H5, Glc–H5), 3.49 (m, 1H, Gal–H4), 3.32 (m, 1H, GalNAc–H2), 2.82 (dd, *J* = 4.57, 12.8 Hz, 1H, Neu5Ac–H3a), 2.21–1.78 (m, 42H, OAc, NHAc), 1.72 (t, *J* = 12.7 Hz, Neu5Ac–H3b). $^{13}$C–NMR (150 MHz, $CDCl_3$, 300 K): δ = 172.1, 171.0, 170.2, 168.8, 100.5, 99.03, 84.75, 76.23, 73.84, 73.53, 72,86, 72.47, 72.23, 71.79, 70.24, 69.73, 68.70, 68.39, 67.56, 66.91, 63.39, 62.62, 62.16, 61.52, 53.23, 52.88, 49.49, 37.39, 23.57, 23.24, 21.56, 21.01, 20.72. HRMS (FAB): Calcd for $C_{56}H_{80}N_3O_{35}$ [$M^+$]: 1353.4494; Found: 1354.4568.

**Preparation of compound 4:**

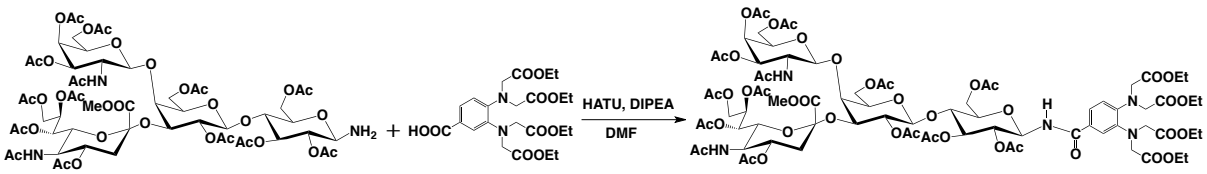


**3** **5** **4**

Compound **5** (250.8 mg, 0.5 mmol) [5], DIPEA (1 mL, 5.7 mmol), and HATU (240 mg, 0.62 mmol) were dissolved in DMF (5 mL), and the mixture was stirred at RT for 10 min. Subsequently, the mixture was transferred to a solution of compound **3** (400 mg, 0.30 mmol) and DIPEA (100 μL, 0.57 mmol) in DMF (1 mL), and this solution was stirred at RT for 12 h. The reaction mixture extracted with EtOAc was washed with $H_2O$, dried with $Na_2SO_4$, and concentrated. The residue was purified on a silica gel column with $CHCl_3$/MeOH (25:1) to give **4** (232 mg, 43%). $^1$H–NMR (600 MHz, $CDCl_3$, 300 K): δ = 7.51 (d, J = 2.08 Hz, 1H, Ar–H), 7.26 (1H, Ar–H), 6.99 (d, *J* = 8.24 Hz, Ar–H), 6.83 (d, *J* = 9.02 Hz, 1H, CONH), 6.21 (d, *J* = 6.88 Hz, 1H, GalNAc–NH), 5.9 (dd, *J* = 3.43, 11.0 Hz, 1H, GalNAc–H3), 5.49 (m, 1H, Neu5Ac–H8), 5.39 (dd, *J* = 2.76, 9.62 Hz, 1H, Neu5Ac–H7), 5.34 (d, *J* = 3.43 Hz, 1H, GalNAc–H4), 5.31 (m, 2H, Glc–H3, Glc–H1), 5.16 (d, *J* = 8.13 Hz, 1H, GalNac–H1), 5.05 (d, *J* = 10.3 Hz, 1H Neu5Ac–NH), 4.96 (m, 2H, Gal–H2, Glc–H2), 4.82 (m, 1H, Neu5Ac–H4), 4.56 (d, *J* = 8.23, 1H, Gal–H1), 4.44–4.19 (m, 12H, Glc–H6a, Neu5Ac–H9a, GalNAc–

H6a, Gal–H4, tag–$NCH_2$), 4.1 (m, 11H, Glc–H6b, GalNAc–H6b, Gal–H6a, $COOCH_2$), 4.04–3.93 (m, 3H, Neu5Ac–H5, Neu5Ac–H9b, Gal–H6b), 3.86–3.74 (m, 7H, Glc–H4, Glc–H5, Gal–H5, Neu5Ac–H6, Neu5Ac–$COOCH_3$), 3.60 (t, $J$ = 6.00 Hz, 1H, GalNAc–H5), 3.50 (d, $J$ = 2.04 Hz, 1H, Gal–H4), 3.33 (m, 1H, GalNAc–H2), 2.83 (dd, $J$ = 4.15, 13.1 Hz, 1H, Neu5Ac–H3a), 2.21–1.83 (m, 42H, OAc, NHAc), 1.74 (m, 1H, Neu5Ac–H3b), 1.18 (m, 12H, tag–$CH_3$). $^{13}$C–NMR (150 MHz, $CDCl_3$, 300 K): δ = 173.4, 172.1, 170.9, 170.0, 168.5, 167.1, 163.1, 145.9, 141.6, 127.7, 122.1, 121.7, 120.8, 100.4, 99.05, 79.00, 75.72, 74.56, 73.56, 72.83, 72.70, 72.20, 71.77, 71.08, 70.25, 69.74, 68.71, 68.35, 67.59, 66.91, 63.39, 62.07, 61.54, 60.72, 53.30, 52.92, 52.22, 49.50, 37.32, 23.50, 23.24, 21.59, 20.98, 20.78, 14.19. HRMS (FAB): Calcd for $C_{79}H_{110}N_5O_{44}$ [M+$H^+$]: 1832.6445; Found: 1832.6515.

**Preparation of the GM2 tetrasaccharide with the tag:**

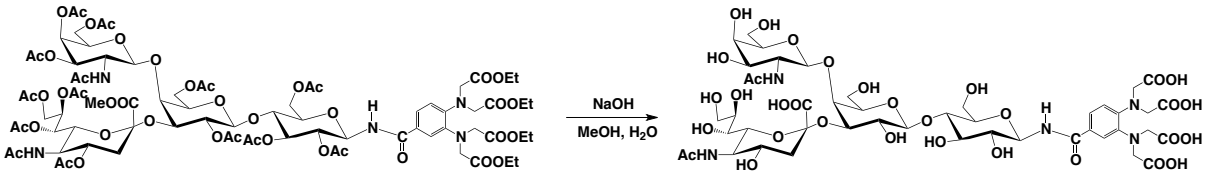


**4** **6**

Compound **4** (100 mg) was dissolved in MeOH and small aliquots of a 1 M NaOH aqueous solution were added until the reaction was complete (checked by TLC). The reaction mixture was purified on an ODS column to give **6** (52 mg, 79%). $^1$H–NMR (600 MHz, $D_2O$, 300 K): δ = 7.29 (m, 2H, Ar–H), 6.79 (d, $J$ = 8.77 Hz, 1H, Ar–H), 5.08 (d, $J$ = 9.36 Hz, 1H, Glc–H1), 4.66 (1H, GalNAc–H1), 4.47 (d, $J$ = 7.68 Hz, Gal–H1), 4.02–4.12 (m, 6H, $NHCH_2$, Gal–H3, Gal–H4), 3.91 (s, 4H, $NHCH_2$), 3.86–3.82 (m, 3H, GalNAc–H4, Glc–H6a, GalNAc–H2), 3.78 (m, 1H, Neu5Ac–H9a), 3.74 (m, 2H, Glc–H6b, Gal–H6a), 3.71–3.66 (m, 7H, Gal–H6b, GalNAc–H6, Neu5Ac–H5, Neu5Ac–H4, Neu5Ac–H8, Gal–H5), 3.62 (m, 4H, GalNAc–H5, Glc–H3, Glc–H5, Glc–H4), 3.58 (dd, $J$ = 3.40 Hz, 10.7, 1H, GalNAc–H3), 3.55–3.48 (m, 3H, Neu5Ac–H9b, Neu5Ac–H7, Glc–H2), 3.38 (d, $J$ = 10.6 Hz, Neu5Ac–H6), 3.29 (t, $J$ = 8.86

Hz, Gal–H2), 2.57 (dd, *J* = 4.02, 12.7 Hz, Neu5Ac–H3a), 1.93 (6H, NHAc), 1.83 (t, *J* = 11.7 Hz, 1H, Neu5Ac–H3b). $^{13}$C–NMR (150 MHz, $D_2O$, 300 K): 182.2, 179.8, 175.6, 172.3, 146.1, 140.3, 124.4, 121.9, 119.6, 118.4, 102.8, 80.07, 78.20, 77.06, 76.51, 74.93, 74.38, 73.30, 72.15, 71.55, 69.97, 68.89, 68.29, 67.85, 62.89, 61.09, 60.06, 54.61, 52.49, 51.89, 37.20, 22.43.

### 3.4.3.2 Preparation of the Tagged GM1 pentasaccharide

**Preparation of the GM1 pentasaccharide:**

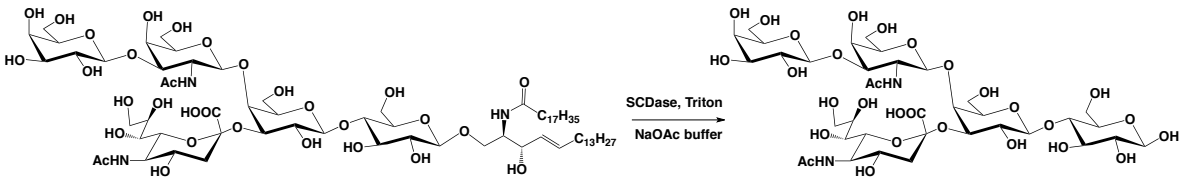


**7**

100 mU Sphingolipid ceramide N–deacylase (SCDase) was added to 10 mL plastic centrifuge tube containing 30 mg GM1 in 2 mL 50 mM NaOAc (pH 6.5) with 0.8% Triton–100. After that, 7 mL decane was added slightly to the top of aqueous solution and kept the reaction in 37 °C for 16 h. Removed the decane completely and heated at 70°C for 5 min and then dried the mixture using centrifugal evaporator. Finally, the mixture was applied to an ODS column to give GM1 pentasaccharide (9 mg). $^{1}$H–NMR (800 MHz, $D_2O$, 300 K). δ = 4.71 (1H, GalNAc–H1), 4.65 (d, *J* = 7.68 Hz, 1H, GalI–H1) 4.59 (1H, Glc–H1), 4.47 (1H, GalII–H1), 4.09 (2H, GalNAc–H4, GalI–H3), 4.06 (1H, GalI–H4), 3.97 (1H, GalNac–H2), 3.89 (1H, Glc–6a), 3.84 (1H, GalII–H4), 3.78 (2H, Glc–6Hb, Neu5Ac–9b), 3.74 (3H, GalNAc–H3, Neu5Ac–H5, GalI–6a), 3.71 (1H, GalI–6b), 3.70 (3H, Neu5Ac–H4, GalNAc–6H), 3.67 (3H, GalI–H5, GalII–6a, Neu5Ac–H8), 3.61 (2H, GalII–H5, GalII–6b), 3.58 (1H, GalNAc–H5), 3.56 (3H, GalII–H3, Glc–H4, Neu5Ac–9a), 3.52 (3H, Glc–H3, Glc–H2, Neu5Ac–H7), 3.42 (2H, Neu5Ac–H6, GalII–H2), 3.20 (1H, Glc–H5), 3.28 (1H, GalI–H2), 2.59 (dd, *J* = 4.02 Hz,

1H, Neu5Ac–3a), 1.95 (3H, GalNAc–H8), 1.94 (3H, Neu5Ac–H11), 1.86 (t, *J* = 11.7 Hz, 1H, Neu5Ac–H3b). $^{13}$C–NMR (800 MHz, $D_2O$, 300 K): 104.8, 102.4, 102.4, 95.77, 80.30, 78.47, 77.14, 74.86, 74.79, 74.29, 74.28, 74.17, 73.57, 72.99, 72.48, 72.24, 71.11, 70.69, 70.00, 68.68, 68.56, 68.03, 67.891, 62.79, 62.78, 61.22, 61.05, 61.0, 60.61, 60.59, 59.86, 59.83, 51.58, 51.18, 36.92, 22.05, 22.65.

**Preparation of the tagged GM1 pentasaccharide:**

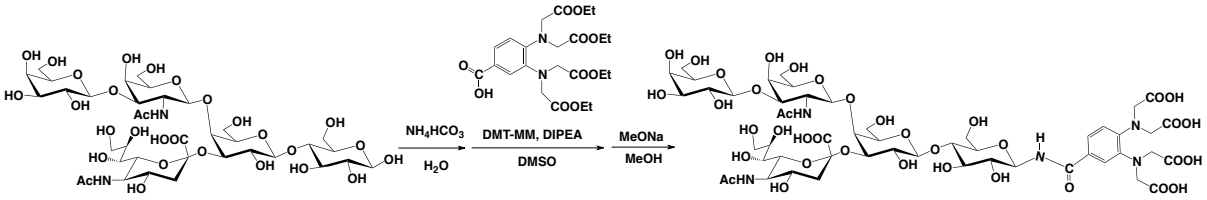


**7** **8**

9 mg GM1 pentasaccharide and excess $NH_4HCO_3$ (around 2–3 g) was dissolved in 2 mL $H_2O$ and kept the reaction for 2d. Then the $H_2O$ and excess $NH_4HCO_3$ was removed by rotary evaporator at 30 °C. After drying, the mixture of tag, DMT–MM and DIPEA in 1 mL DMSO was added. The reaction was kept for all night. Add 10 mL H2O to dilute the reaction mixture and then applied to ODS column to get tagged–GM1. The deprotection of tag part was done by dissolve the sample in to 2 mL MeOH containing MeONa. The reaction was stirred for 4 h and then purified using by Sephadex G–10 column to remove the salt. 1H–NMR (800 MHz, D2O, 300 K). δ = 7.35 (m, 2H, Ar–H), 6.85 (d, *J* = 8.77 Hz, 1H, Ar–H), 5.14 (1H, Glc–H1), 4.71 (1H, GalNAc–H1), 4.89 (d, J = 7.68 Hz, 1H, GalI–H1) 4.47 (1H, GalII–H1), 4.09 (3H, GalNAc–H4, GalI–H3, GalI–H4), 3.97 (1H, GalNAc–H2), 3.89 (2H, Glc–6a, GalII–H4), 3.79 (5H, Glc–6Hb, Neu5Ac–9b, GalNAc–H3, Neu5Ac–H5, GalI–6a), 3.71 (6H, GalI–6b, Neu5Ac–H4, GalNAc–6H, GalI–H5, Glc–H3), 3.68 (5H, GalII–6a, Neu5Ac–H8, GalNAc–H5, Glc–H4, Glc–H5), 3.61 (2H, GalII–H5, GalII–6b), 3.56 (2H, GalII–H3, Neu5Ac–9a), 3.54 (1H, Glc–H2), 3.51 (1H, Neu5Ac–H7), 3.42 (2H, Neu5Ac–H6, GalII–H2), 3.28 (1H, GalI–H2), 2.59 (dd, *J* = 4.02, 1H, Neu5Ac–3a), 1.95 (3H, GalNAc–H8), 1.94 (3H, Neu5Ac–

H11), 1.86 (t, $J$ = 11.7 Hz, 1H, Neu5Ac–H3b). $^{13}$C–NMR (150 MHz, $D_2O$, 300 K): 104.8, 102.4, 102.4, 80.32, 79.81, 77.81, 77.14, 76.53, 75.03, 74.86, 74.28, 74.07, 72.99, 72.48, 72.24, 71.35, 70.69, 70.00, 68.68, 68.56, 68.03, 67.89, 62.79, 62.78, 61.22, 61.05, 60.97, 60.61, 60.59, 59.86, 59.83, 51.58, 51.18, 36.91, 22.65, 22.05.

### 3.4.4 PCS observation and analyses

Tagged GM2 tetrasaccharide (compound 6) or tagged GM1 pentasaccharide (compound 8) was dissolved in $D_2O$ (0.25 mL) and the pH was increased to 8.0 by adding a solution of NaOD. This solution was titrated with a $D_2O$ solution of $MCl_3$ (250 mM; M = $La^{3+}$, $Tm^{3+}$, or $Tb^{3+}$) for the NMR measurements. For the PCS observations, $^{1}$H–$^{13}$C HSQC spectra were recorded at 300 K with 512 ($t_1$) and 1024 ($t_2$) complex points. The NMR spectra were processed and analyzed with the NMRPipe [16] and Sparky [17] programs.

Two thousand conformers were extracted from the combined trajectory of the GM2 tetrasaccharide every 50 ps, and the averaged paramagnetic center defined from additional MD calculations of the tag moiety [5] was added by aligning each glucose ring. A single $\Delta\chi$ tensor was determined for the conformational ensemble by inspection of the experimentally obtained PCSs with the assumption that every conformer contributes equally to the PCSs by a modified version of MSpin [18].

## References:


1. **(a)** M. R. Wormald, A. J. Petrescu, Y. L. Pao, A. Glithero, T. Elliott and R. A. Dwek, Conformational studies of oligosaccharides and glycopeptides: complementarity of NMR, X–ray crystallography, and molecular modelling. *Chem. Rev.,*102 (**2002**) 371–386. **(b)** Y. Kamiya, M. Yagi–Utsumi, H. Yagi and K. Kato, Structural and molecular

basis of carbohydrate–protein interaction systems as potential therapeutic targets. *Curr. Pharm. Des*., 17 (**2011**) 1672–1684.

2. K. Kato, Y. Kamiya, Structural views of glycoprotein–fate determination in cells. *Glycobiology 17* (**2007**) 1031–1044.

3. **(a)** L. Ellgaard, A. Helenius, Quality control in the endoplasmic reticulum, *Nat. Rev. Mol. Cell Biol.* 4 (**2003**) 181–191. **(b)** Y. Kamiya, K. Kato, Sugar recognition by intracellular lectins that determine the fates of glycoproteins, *Trends Glycosci. Glycotechnol.* 18 (**2006**) 231–244. **(c)** T. Anelli, R. Sitia, Protein quality control in the early secretory pathway, *EMBO J.* 27 (**2008**) 315–327. **(d)** Y. Kamiya, D. Kamiya, R. Urade, T. Suzuki, K. Kato, Sophisticated modes of sugar recognition by intracellular lectins involved in quality control of glycoproteins, *Nova Science Publisher, Inc., N.Y.,* **2009. (e)** Y. Takeda, K. Totani, I. Matsuo, Y. Ito, Chemical approaches toward understanding glycan–mediated protein quality control, *Curr. Opin. Chem. Biol*. 13 (**2009**) 582–591. **(f)** G. Z. Lederkremer, Glycoprotein folding, quality control and ER–associated degradation, *Curr. Opin. Struct. Biol.* 19 (**2009**) 515–523. **(g)** M. Aebi, R. Bernasconi, S. Clerc, M. Molinari, N–glycan structures: recognition and processing in the ER, *Trends Biochem. Sci.* 35 (**2010**) 74–82.

4. Y. Kamiya, T. Satoh, K. Kato, Molecular and structural basis for N–glycan–dependent determination of glycoprotein fates in cells, *Biochim Biophys Acta.* 1820 (**2012**) 1327–37.

5. S. Yamamoto, Y. Zhang, T. Yamaguchi, T. Kameda, K. Kato, Lanthanide–assisted NMR evaluation of a dynamic ensemble of oligosaccharide conformations. *Chem. Commun.* 48 (**2012**) 4752–4754.

6. K. N. Kirschner, A. B. Yongye, S. M. Tschampel, J. Gonzalez–Outeirino, C. R. Daniels, B. L.Foley, R. J. Woods, GLYCAM06: A generalizable biomolecular force field. Carbohydrates. *J. Comput. Chem.* 29 (**2008**) 622–655.

7. **(a)** Y.T.; Li, S. C. Li, A. Hasegawa, H. Ishida, M. Kiso, A. Bernardi, P. Brocca, L. Raimondi, S. Sonnino, Structural basis for the resistance of Tay–Sachs ganglioside GM2 to enzymatic degradation. *J. Biol. Chem.* 274 (**1999**) 10014–10018. **(b)** K. Veluraja, V. S. R. Rao, Theoretical studies on the conformation of monosialogangliosides and disialogangliosides. *Carbohydr. Polym.* 3 (**1983**) 175–192. **(c)** S. Sabesan, K. Bock, U. Lemieux, The conformational properties of the ganglioside GM2 and GM1 based on $^{1}H$ and $^{13}C$ nuclear magnetic resonance studies. *Can. J. Chem*. 62 (**1984**) 1034–1045. **(d)** P. Brocca, A. Bernardi, L. Raimondi, S. Sonnino, Modeling ganglioside headgroups by conformational analysis and molecular dynamics. *Glycoconj. J.* 17 (**2000**) 283–299. **(e)** K. Veluraja, J.F.A. Selvin, S. Venkateshwari, T.R.K. Priyadarzini, 3DSDSCAR–a three dimensional structural database for sialic acid–containing carbohydrates through molecular dynamics simulation. *Carbohydr. Res.* 345 (**2010**) 2030–2037.

8. **(a)** S. Re, W. Nishima, N. Miyashita and Y. Sugita, Conformational flexibility of N–glycans in solution studied by REMD simulations, *Biophys Rev* 4 (**2012**) 179–187. **(b)** S. Re, N. Miyashita, Y. Yamaguchi, Y. Sugita, Structural diversity and changes in conformational equilibria of biantennary complextype N–glycans in water revealed by replica–exchange molecular dynamics simulation. *Biophys J* 101 (**2011**) L44–L46. **(c)** W. Nishima, N. Miyashita, Y. Yamaguchi, Y. Sugita, S. Re, Effect of bisecting GlcNAc and core fucosylation on conformational properties of biantennary complex–type N–glycans in solution. *J Phys Chem* 116 (**2012**) 8504–8512.

9. S.B. Levery, $^{1}$H–NMR study of GM2 ganglioside: Evidence that an interresidue amide–carboxyl hydrogen bond contributes to stabilization of a preferred conformation. *Glycoconj. J.* 8 (**1991**) 484–92.

10. T.A.W. Jr. Koerner, J.H. Prestigard, P.C. Demou, R.K. Yu, High–resolution proton NMR studies of gangliosides. 1. Use of homonuclear two–dimensional spin–echo J–correlated spectroscopy for determination of residue composition and anomeric configurations. *Biochemistry* 22 (**1983**) 2676–2687.

11. D.A. Case, T.A. Darden, T.E. Cheatham, C.L. Simmerling, J. Wang, R.E. Duke, R. Luo, R.C. Walker, W. Zhang, K.M. Merz, B.P. Roberts, B. Wang, S. Hayik, A. Roitberg, G. Seabra, I. Kolossvai, K.F. Wong, F. Paesani, J. Vanicek, J. Liu, X. Wu, S.R. Brozell, T. Steinbrecher, H. Gohlke, Q. Cai, X. Ye, J. Wang, M.J. Hsieh, G. Cui, D.R. Roe, D.H. Mathews, M.G. Seetin, C. Sagui, V. Babin, T. Luchko, S. Gusarov, A. Kovalenko, P.A. Kollman, Amber11, *University of California, San Francisco, CA, USA,* **2010**.

12. H.J.C. Berendsen, J.P.M. Postma, W.F.V. Gunsteren, A. DiNola, J.R. Haak, Molecular dynamics with coupling to an external bath. *J. Chem. Phys.* 81 (**1984**) 3684–3691.

13. J.P. Ryckaert, G. Ciccotti, H.J.C. Berendsen, Numerical integration of the cartesian equations of motion of a system with constraints: molecular dynamics of n–alkanes. *J. Comput. Phys.* 23 (**1977**) 327–341.

14. T. Darden, D. York, L. Pedersen, Particle mesh Ewald: An N·log(N) method for Ewald sums in large systems. *J. Chem. Phys.* 98 (**1993**) 10089–10092.

15. W. Humphrey, A. Dalke, K. Schulten, VMD–visual molecular dynamics. *J. Molec. Graphics.* 14 (**1996**) 33–38.

16. F. Delaglio, S. Grzesiek, G.W. Vuister, G. Zhu, J. Pfeifer, A. Bax, NMRPipe: A multidimensional spectral processing system based on UNIX pipes. *J. Biomol. NMR* 6 (**1995**) 277–293.

17. T.D. Goddard, D.G. Kneller, SPARKY 3; University of California, San Francisco.

18. V.M. Sánchez–Pedregal, R. Santamaría–Fernández, A. Navarro–Vázquez, Residual dipolar couplings of freely rotating groups in small molecules. stereochemical assignment and side–chain conformation of 8–phenylmenthol. *Org. Lett.* 11 (**2009**) 1471–1474.

# Chapter 4. Summary and Perspective

Characterization of the conformational dynamics of oligosaccharides is a pivotal step to understand the underlying mechanisms of their functions in living system. Although NMR is powerful method for elucidating the atomic details of biomolecules, the local distance restraints given by NOE and *J* coupling are normally not sufficient to provide the 3D structural information for understanding the detailed conformations of oligosaccharides. PCS, a paramagnetic effect exhibiting as chemical shift changes due to dipole–dipole interactions between nuclei and an unpaired electron, is appropriate for providing the long–distance information of the overall structures of oligosaccharides. However, the experimental data should be evaluated as the conformational ensemble because of the conformational flexibility of oligosaccharides. Computational simulation is potent to provide the 3D structural ensemble model of flexible molecules, but simulation results depend on several parameters such as force field, initial structure and simulation time. Therefore, the experimental data for validating the simulation result is essential. In view of these situations, I have developed a systematic method for conformational dynamics analyses of oligosaccharides by combining computational simulations and PCS observations.

For obtaining the PCSs, a phenylenediamine–based lanthanide–chelating tag was designed for introducing the paramagnetic probe into oligosaccharides. The rigidity of the tag was crucial for successful observation of PCS and unambiguous interpretation of the data. The synthesized tag was covalently attached to the reducing end of a series of ganglioside glycans, GM3, GM2 and GM1 oligosaccharides through rigid amide bond. Upon chelating with paramagnetic lanthanide ions, the tagged oligosaccharides exhibited NMR spectral changes, thereby offering an opportunity to determine the spatial positions of the individual $^{1}H$ and $^{13}C$ nuclei with respect to the paramagnetic metal center. For construction of the 3D structural model, all–atom MD simulations of these oligosaccharides were employed. The cooperation of the experimental PCS data and the computational simulation results

successfully provided the conformational ensembles of linear GM3 trisaccharide, branched GM2 tetrasaccharide and GM1 pentasaccharide. The PCS analyses exhibited as a powerful tool for validating the authenticity of the dynamic conformations of the glycans due to possible discrepancy of simulation results caused by insufficient structure sampling.

By comparing the obtained conformational ensembles of GM1 pentasaccharide, GM2 tetrasaccharide and GM3 trisaccharide, the consistence and difference of the 3D structure and dynamics of these glycans were clearly revealed. The data showed that GM1 pentasaccharide and GM2 tetrasaccharide shared the similar conformational space, which indicates the additional Gal residue does not affect the conformation of inner part of GM1 pentasaccharide. On the other hand, the additional GalNAc residue in branched GM2 induced significant different conformations of the Neu5Ac–Gal glycosidic linkage from those of linear GM3 trisaccharide as found in both simulation and experimental results. Furthermore, it was identified that the inter–branch interactions between GalNAc and Neu5Ac residues are responsible for the unique conformations of Neu5Ac–Gal linkage in GM2. These results indicated that the paramagnetism–assisted NMR in conjunction with MD simulation is powerful method to characterize the conformational dynamics of flexible and branched oligosaccharides.

This methodology opens a new prospect for conformational analyses of dynamic structures of glycans toward decoding glycocodes from the 3D structural aspects, giving mechanistic insights into their various physiological and pathological roles in living system. It is potent to provide the 3D structure ensemble of not only oligosaccharides but also other highly flexible biomolecules such as intrinsically disordered proteins. However, compared to protein structural biology, the NMR analyses of glycans are still immature. For example, characterization of structural basis of oligosaccharide interactions remains a challenging task. To address this issue, several NMR techniques such as saturation–transfer difference

measurement have been developed [1]. Paramagnetic NMR approaches are also useful to detect the weak interaction of oligosaccharides and determine their multiple structures in complexes [2].

Formation of clusters as exemplified by glycolipids on cell surface is another unique feature of oligosaccharides in addition to conformational flexibility. The oligosaccharide clusters serve as a unique platform for specific interactions of various biomolecules [3]. Although the detailed information on interactions between glycolipids in the clusters is quite important to uncover the underlying mechanisms of their functions, atomic level description of carbohydrate–carbohydrate interactions is a still challenging task. Characterization of the dynamics of the glycolipid clusters involves not only precise analyses of the conformational ensemble of each constituent but also the cooperative action of the glycolipids.

Paramagnetic NMR in conjunction with large–scale MD simulations is the potential method that can characterize the conformational dynamics and interactions of glycolipid clusters. However, due to poor chemical shift dispersion of glycolipids because of their less divergence of functional groups, low–resolution of NMR spectra is frequently big issue, which hinders the unambiguous peak assignment and detailed analyses [4]. One of the useful approaches for solving this issue is selective and/or uniform stable isotope–labeling of the samples. Uniformly $^{13}C$–labeled oligosaccharides using eukaryotic cells and genetically engineered yeast cells have been reported [5]. Several disaccharides and trisaccharides with stable isotope–labeling also have been synthesized by using chemical methods [6]. The systematic techniques for preparation of glycolipids possessing a large oligosaccharide moiety with position–selective isotope–labeling has been developing.

In addition, appropriate membrane–mimicking system for NMR measurements is also critical for effective elucidation of the dynamics and interactions of glycolipid clusters. A number of membrane mimics such as micelles, nanodiscs and bicelles have been used for

NMR measurements [7]. For example, ganglioside–embedding small bicelles have recently been proposed as nanoscale standardized membrane mimics for the detailed NMR analysis of interactions between ganglioside clusters and biomolecules, including intrinsically disordered proteins associated with neurodegenerative disorders [8].

Glycolipid cluster is an interesting and also challenging system to be analyzed. By employing multidisciplinary approaches based on paramagnetism–assisted NMR, computational simulation, isotope–labeled sample synthesis, and membrane model design, the dynamics and corporative actions of the glycolipids on cell membrane will be reveled.

**References:**


1. A. Ardá, P. Blasco, D. V. Silva, V. Schubert, S. André, M. Bruix, F. J. Cañada, H. J. Gabius, C. Unverzagt, J. Jiménez– Barbero, Molecular recognition of complex–type biantennary N–glycans by protein receptors: a three–dimensional view on epitope selection by NMR, *J. Am. Chem. Soc.* 135 (**2013**) 2667–2675.
2. T. Zhuang, H. S. Lee, B. Imperiali, J. H. Prestegard, Structure determination of a Galectin–3–carbohydrate complex using paramagnetism–based NMR constraints, *Protein Sci*. 17 (**2008**) 1220–1231.
3. **(a)** M. Yagi–Utsumi, T. Kameda, Y. Yamaguchi, K. Kato, NMR characterization of the interactions between lyso–GM1 aqueous micelles and amyloid beta, *FEBS Lett.,* 584 (**2010**) 831–836. **(b)** M. Utsumi, Y. Yamaguchi, H. Sasakawa, N. Yamamoto, K. Yanagisawa, K. Kato, Up–and–down topological mode of amyloid β–peptide lying on hydrophilic/hydrophobic interface of ganglioside clusters, *Glycoconj. J.* 26 (**2009**) 999–1006.

4. L. Mauri, R. Casellato, M. G. Ciampa, Y. Uekusa, K. Kato, K Kaida, M. Motoyama, S. Kusunoki, and S. Sonnino, Anti–GM1/GD1a complex antibodies in GBS sera specifically recognize the hybrid dimer GM1–GD1a, *Glycobiology* 22 (**2012**) 352–360.

5. **(a)** K. Kato, Y. Yamaguchi, Y. Arata, Stable–isotope–assisted NMR approaches to glycoproteins using immunoglobulin G as a model system, *Prog. Nucl. Magn. Reson. Spectrosc*. 56 (**2010**) 346–359. **(b)** Y. Yamaguchi, K. Kato, Dynamics and interactions of glycoconjugates probed by stable–isotope–assisted NMR spectroscopy, *Methods Enzymol*. 478 (**2010**) 305–322. **(c)** V. Blanchard, R. A. Gadkari, A. V. E. George, S. Roy, G. J. Gerwig, B. R. Leeflang, R. R. Dighe, R. Boelens, J. P. Kamerling, High–level expression of biologically active glycoprotein hormones in Pichia pastoris strains–selection of strain GS115, and not X–33, for the production of biologically active N–glycosylated $^{15}$N–labeled phCG, *Glycoconj J*. 25 (**2008**) 245–257. **(d)** W. J. Walton, A. J. Kasprzak, J. T. Hare, T. M. Logan, An economic approach to isotopic enrichment of glycoproteins expressed from Sf9 insect cells, *J. Biomol. NMR* 36 (**2006**) 225–233. **(e)** Y. Kamiya, S. Yamamoto, Y. Chiba, Y. Jigami, K. Kato, Overexpression of a homogeneous oligosaccharide with 13C labeling by genetically engineered yeast strain, *J. Biomol. NMR* 50 (**2011**) 397–401.

6. **(a)** J. M. Duker, A. S. Serianni, ($^{13}$C)–substituted sucrose: $^{13}$C–$^{1}$H and $^{13}$C–$^{13}$C spin coupling constants to assess furanose ring and glycosidic bond conformations in aqueous solution, *Carbohydr. Res.* 249 (**1993**) 281–303. **(b)** B. Bose, S. Zhao, R. Stenutz, F. Cloran, P. B. Bondo, G. Bondo, B. Hertz, I. Carmichael, A. S. Serianni, Three–bond C–O–C–C spin–coupling constants in carbohydrates: development of a Karplus relationship, *J. Am. Chem. Soc.* 120 (**1998**) 11158–11173. **(c)** U. Olsson, A. S. Serianni, R. Stenutz, Conformational analysis of beta–glycosidic linkages in $^{13}$C–labeled glucobiosides using inter–residue scalar coupling constants, *J. Phys. Chem. B*

112 (**2008**) 4447–4453. **(d)** K. H. M. Jonsson, R. Pendrill, G. Widmalm, NMR analysis of conformationally dependent $^{n}J_{C,\ H}$ and $^{n}J_{C,\ C}$ in the trisaccharide α–L–Rhap–(1→2)[α–L–Rhap–(1→3)]–α–L–Rhap–OMe and a site–specifically labeled isotopologue thereof, *Magn. Reson. Chem.* 49 (**2011**) 117–124. **(e)** K. H. M. Jonsson, E. Säwén, G. Widmalm, Studies on the conformational flexibility of α–L–rhamnose–containing oligosaccharides using $^{13}C$–site–specific labeling, NMR spectroscopy and molecular simulations: implications for the three–dimensional structure of bacterial rhamnan polysaccharides, *Org. Biomol. Chem*. 10 (**2012**) 2453–2463.

7. E. Serebryany, G. Alex Zhu, E. C.Y. Yan, Artificial membrane–like environments for in vitro studies of purified G–protein coupled receptors, *Biochimica et Biophysica Acta* 1818 (**2012**) 225–233.
8. T. Yamaguchi, T. Uno, Y. Uekusa, M. Yagi–Utsumi, K. Kato, Ganglioside–embedding small bicelles for probing membrane–landing processes of intrinsically disordered proteins, *Chem. Commun.* 49 (**2013**) 1235–1237.

# Acknowledgments

First and foremost, I would like to express my heartfelt gratitude to my PhD advisor, Prof. Koichi Kato for accepting me into this wonderful group and for his guidance and support throughout my PhD. His outstanding knowledge and brilliant sense on science as well as his willingness to transfer it to us set me an excellent role model for being a scientist and professor. I am very grateful for all his time that he took to have discussion with me on our work, to have rehearsal for my presentation, to have my presentation slides and documents improved, even during his busy schedule. I am also very grateful to Dr. Takumi Yamaguchi for his immense help for teaching me the experimental skill such as chemical synthesis, NMR measurement and simulation, sharing his abundant scientific knowledge and giving me the insightful discussion when the experiment went tough. Thanks for improving documents for me once and once again even during the holiday.

I would like to thank Dr. Yokiko Kamiya for teaching me the experiment about protein expression and purification. I also thank Dr. Yoshinori Uekusa for teaching the processing of NMR data by using nmrpipe, Sparky and ccpnmr. Thanks to Dr. Maho Yagi–Utsumi for her brilliant opinion on discussion of my research work and presentations. Thanks to Ms. Sayoko Yamamoto for her contribution to MD simulation of oligosaccharide. Thanks to Dr. Tomoshi Kameda (Advanced Industrial Science and Technology, Dr. Yoshitake Sakae (Nagoya University), Dr. Yuko Okamoto (Nagoya University) for the useful discussion and cooperation on simulation. Thanks to Dr. Kotaro Yanagi and Dr. Ying-hui Wang for sharing the knowledge of NMR. Thanks to Dr. Hirokazu Yagi and Dr. Tadashi Satoh for sharing the knowledge of biological science. Thanks to all these excellent scientists for the immense help and thus make my PhD experience productive.

I always consider myself extremely lucky that I had a chance to work with so many good teachers and helpful friends. Thanks to Kentaro Kumoi and Keisuke Okawa for their

niceness and sense of humor. Thanks to Kouya Inagaki for the drink party and his beautiful song. Thanks to Tong Zhu, Ratsupa Thammaporn, Arunima Sikdar for our sincere friendship and sharing the great time together. Thanks to Jingzheng Wang, Gengwei Yan and Pa Padungros for sharing the experimental room, great time and solving the experimental problem together. Thanks to previous visitors, Aoy Pornthip, Darren Gouk for the great time we shared. Thanks to all of them for their encouragement, accompany during my PhD.

I sincerely appreciate the examiners of this thesis Prof. Shigetoshi Aono, Prof. Koichi Fukase, Prof. Hisashi Okumura, Prof. Katsuyuki Nishimura for their precious time and valuable comments.

Lastly, I especially thank my mom, my dad, my sibling and my husband for their great support, unconditionally love and immense encouragement all the time.